



# Aerosol processing and CCN formation of an intense Saharan dust plume during the EUCAARI 2008 campaign

Nelson Bègue, Pierre Tulet, Jacques Pelon, B. Aouizerats, A. Berger, Alfons Schwarzenboeck

## ► To cite this version:

Nelson Bègue, Pierre Tulet, Jacques Pelon, B. Aouizerats, A. Berger, et al.. Aerosol processing and CCN formation of an intense Saharan dust plume during the EUCAARI 2008 campaign. *Atmospheric Chemistry and Physics*, 2015, 15, pp.3497-3516. 10.5194/acp-15-3497-2015 . hal-01078326

**HAL Id: hal-01078326**

**<https://hal.science/hal-01078326>**

Submitted on 2 Apr 2015

**HAL** is a multi-disciplinary open access archive for the deposit and dissemination of scientific research documents, whether they are published or not. The documents may come from teaching and research institutions in France or abroad, or from public or private research centers.

L'archive ouverte pluridisciplinaire **HAL**, est destinée au dépôt et à la diffusion de documents scientifiques de niveau recherche, publiés ou non, émanant des établissements d'enseignement et de recherche français ou étrangers, des laboratoires publics ou privés.



# Aerosol processing and CCN formation of an intense Saharan dust plume during the EUCAARI 2008 campaign

N. Bègue<sup>1</sup>, P. Tulet<sup>1</sup>, J. Pelon<sup>2</sup>, B. Aouizerats<sup>3</sup>, A. Berger<sup>4</sup>, and A. Schwarzenboeck<sup>5</sup>

<sup>1</sup>Laboratoire de l'Atmosphère et des Cyclones, UMR 8105 CNRS, University of Réunion Island, Reunion Island, France

<sup>2</sup>Laboratoire Atmosphère Milieux Observations Spatiales, University of Paris VI, Paris, France

<sup>3</sup>Faculty of Earth and Life Sciences, VU University Amsterdam, Amsterdam, the Netherlands

<sup>4</sup>Laboratoire d'Aérodynamique, University of Paul Sabatier, CNRS, Toulouse, France

<sup>5</sup>Laboratoire de Météorologie Physique, CNRS, UMR 6016 University Blaise-Pascal, Clermont-Ferrand, France

Correspondence to: N. Bègue (nelson.begue@univ-reunion.fr)

Received: 18 July 2014 – Published in Atmos. Chem. Phys. Discuss.: 28 October 2014

Revised: 26 February 2015 – Accepted: 10 March 2015 – Published: 31 March 2015

**Abstract.** Atmospheric processing and CCN formation of Saharan dust is illustrated through the analysis of a case of dust transport over northern Europe. This spread of dust is investigated by combining satellite, airborne and ground-based observations and the non-hydrostatic meso-scale model Meso-NH. The altitude of the dust plume during its transport to northwestern Europe was assessed using the CALIPSO observations and our model results. The major dust plume was transported toward Mediterranean and European regions between 2 and 5 km above sea level (a.s.l.). This is confirmed by an average particle depolarization ratio equal to 30 %. Due to transport, this layer split into two layers over northern Europe, and we analyzed in this paper possible mixing of the European pollution aerosol with dust particles in the lower layer. The simulations have shown that the lower dust layer has interacted with the anthropogenic aerosol mainly over Belgium and the Netherlands. The analyses of numerical simulation results show that mineral dust particles accumulated soluble material through internal mixing over the Netherlands. The value of the  $CCN_{0.2}$  / CN ratio obtained over the Netherlands ( $\sim 70\%$ ) is much greater than those observed over the Saharan region. In addition over the Netherlands, the CCN measurement reached 14 000 particles  $cm^{-3}$  at 0.63 % supersaturation level on 30 May. Our model results reveal that more than 70 % of the CCN concentration observed on 30 May can be explained by the presence of Saharan aged dust. The study reveals that heterogeneous reactions with inorganic salts converted this Saharan mineral dust into compounds that were sufficiently soluble

to impact hygroscopic growth and cloud droplet activation over the Netherlands.

## 1 Introduction

Dust aerosol is considered as one of the most plentiful aerosol species in the atmosphere (Engelstaedter et al., 2006; Washington et al., 2006; Penner et al., 2001), and is well known for the role it can play in the climate system by affecting the radiation budget (Koehler et al., 2010; Forster, 2007; Haywood and Boucher, 2000). It is also known that dust may affect biogeochemical cycles, acting as a fertilizer for the ocean (Mohwald et al., 2005; Sarthou et al., 2003; Archer and Johnson, 2000). Dust is involved in heterogeneous, multiphase atmospheric chemistry, affecting photo-oxidant concentrations and the composition of precipitation (Laurent et al., 2008; Bauer et al., 2004). Knowledge of the spatial and temporal distribution of dust aerosol and its properties is therefore crucial to the description of atmospheric processes and their climatic effects. The complexity of the interaction of dust with radiation and the biogeochemical cycle are among the most uncertain factors in climate studies and weather prediction. Although progress has been made in understanding the role of dust in the climate system, some uncertainties are still present (Forster, 2007). For instance, many uncertainties remain regarding the radiative properties and the atmospheric budget for dust (Ansmann et al., 2011; Bauer et al., 2010; Zender et al., 2003; Ginoux et al., 2004).

Numerical models that simulate the processes of dust emission, its chemical and physical transformations and its deposition have improved in recent years to provide a more accurate description of the properties and processes of atmospheric aerosols (Todd et al., 2008). Furthermore, previous studies on the dust source locations and their variability have clearly demonstrated the usefulness of satellite observations in improving models and decreasing the current uncertainties (Tegen et al., 2013; Schepanski et al., 2007).

Dust is mainly produced by the wind erosion acting in arid and semi-arid regions. Half of the world's atmospheric dust originates from the North African deserts, with emissions ranging from 160 to 1600 Tg yr<sup>-1</sup> (Engelstaedter et al., 2006). The Saharan desert with the Sahel region is widely regarded as earth's largest source of dust (Engelstaedter and Washington, 2007; Tanaka and Chiba, 2006). A large part of the North African dust emissions are known to come from the Bodélé depression, which can be activated during cyclonic events (Koehler et al., 2010; Bou Karam et al., 2009; Engelstaedter and Washington, 2007; Schepanski et al., 2007; Washington et al., 2006; Caquineau et al., 2002; Goudie and Middleton, 2001). Because Saharan dust can be transported over long distances in the atmosphere, it can affect natural and human environments far away from its sources. The bulk of Saharan dust is transported westward into the Atlantic Ocean, where it can impact the ecosystems of the American coast (Goudie, 2014; Prospero et al., 2002) and may alter the biogeochemical cycle in the Amazon Basin and Atlantic Ocean (Jickells, 2005; Swap et al., 1992). Europe and the Mediterranean basin can be affected by dust episodes originating in the Saharan region (Pappalardo et al., 2010; Papayannis et al., 2008; Mona et al., 2006; Collaud Coen et al., 2004). Furthermore, in extreme cases, Saharan dust can be transported to northern Europe, reaching the shores of the Baltic Sea (Bègue et al., 2012; Ansmann et al., 2003).

The significant role of dust in providing ice nuclei (IN) has been rather well identified (Chou et al., 2011; Stith et al., 2009; DeMott et al., 2003; Sassen et al., 2003). A few studies have recently reported the ability of dust to act as cloud condensation nuclei (CCN) (Kumar et al., 2011; Koehler et al., 2010, 2009; Sullivan et al., 2009; Kelly et al., 2007; Perry et al., 2004). When dust is emitted, it is often composed of insoluble or only slightly soluble components. During their transport, the dust particles can accumulate soluble material through internal mixing, which drastically reduces the saturation required for activation (Dusek et al., 2006). The dust particles provide reaction sites for heterogeneous chemical reactions with atmospheric trace gases and pollutants that result in modified dust properties, such as enhanced hygroscopicity (Hatch et al., 2008; Levin et al., 1996). Through the analysis of measurements realized in the laboratory, Gibson et al. (2007) shown that the coating of dust enhance significantly their ability to act as CCN. From airborne measurements over Amazon Basin, Roberts et al. (2002) made a detailed sensitivity analysis of CCN spectra on chemical

and physical properties of aerosol. They have shown that a change of 20 % in the amount of soluble material can impact significantly the hygroscopic properties of aerosols that initially contain less soluble material, such as dust. Through the analysis of samples collected during brown haze and dust episode from 24 May to 21 June 2007 in Beijing, Li et al. (2009) have shown that dust particles that acquire hygroscopic nitrate coating tend to be more spherical and larger, enhancing their light scattering and CCN activity. Soluble coatings on dust can be observed in the atmosphere during the event of long-range transport of the plume. Several studies of Asian dust have shown that its atmospheric processing may have a considerable impact on the activation of Asian dust transported over a long range (Stone et al., 2011; Sullivan et al., 2007; Roberts et al., 2006; Perry et al., 2004; Chen et al., 1997). As far as African dust is concerned, significant sulfate coating on transported Saharan dust and an enhancement of the hygroscopic properties of this dust by the coating has been shown over the Mediterranean basin (Levin et al., 2001; Wurzler et al., 2000; Falkovich et al., 2001). Twohy et al. (2009) have shown that Saharan dust commonly acts as CCN over the eastern North Atlantic. To date, only a few studies on the ability of Saharan dust to act as CCN during its transport over northern Europe have been reported. Based on this observation, we present a study of the atmospheric processing of Saharan dust through the analysis of a case of dust transport over northern Europe.

Long-range transport of Saharan dust to northern parts of Europe was observed during the European Integrated project on Aerosol, Cloud, Climate and Air Quality Interactions (EUCAARI) (Kulmala et al., 2009). From 25 to 31 May 2008, an intense Saharan dust plume was transported over Europe and reached the shores of the Baltic Sea. The synoptic analysis reported by Hamburger et al. (2011) revealed that the dust event took place in a meteorological situation characterized by strong convective activity and heavy precipitation associated with the advection of a frontal system over central Europe. This dust event provided the framework for Pappalardo et al. (2010) to show their first results in terms of comparison between lidar measurements obtained from Cloud-Aerosol Lidar and Infrared Pathfinder Satellite Observation (CALIPSO) and the European Aerosol Research Lidar Network (EARLINET). Klein et al. (2010) have shown that the Saharan dust transported during this episode contributed significantly to the abundance and composition of ice nuclei in central Europe. More recently, Bangert et al. (2012) analyzed the impact of the Saharan dust transported on the radiation and cloud formation over western Europe during this dust event of May 2008. Through the use of the regional scale model COSMO-ART, they revealed that, on the one hand, the direct interaction of dust with radiation caused an additional reduction of 40 to 80 W m<sup>-2</sup> in the incoming shortwave radiation, whereas the incoming longwave radiation at the surface increased significantly, by about +10 W m<sup>-2</sup>. On the other hand, they showed that the

number concentration of ice crystals was determined by Saharan dust, due to efficient heterogeneous freezing of the dust. The impacts of the interaction between the Saharan dust plume and convective activity on dust optical properties have also been reported recently by Bègue et al. (2012). Using the meso-scale model Meso-NH, they demonstrated a high precipitation scavenging efficiency for the dust coarse mode, which modified the dust optical characteristics in the measurements recorded over the Netherlands.

The present paper extends the results of the first study of dust plume properties over the Netherlands, carried out by Bègue et al. (2012). The measurements obtained during the EUCAARI campaign reveal a large increase in the number concentration of CCN, coinciding with the transport of Saharan dust over the Netherlands on 30 May 2008. Thus, questions arise about a possible enhancement of the hygroscopicity of the Saharan dust plume by accumulation of soluble material during its transport over the Netherlands. This hypothesis is explored through a methodology combining observations and numerical tools. In this paper, first, the presence of a zone where mixing occurs between the dust plume and European anthropogenic aerosols is examined through an analysis of air mass transport from the emission of the dust aerosols to their arrival over the Netherlands. A second step examines and discusses the influence of the aging of Saharan dust by coating on its hygroscopic properties. We focus particularly on the influence of the chemical composition on the activation of Saharan dust transported over a long range.

The paper is organized as follows: Sect. 2 describes the observations and the model used to investigate the evolution of the dust hygroscopicity; Sect. 3 presents the interaction between the Saharan dust plume and European anthropogenic aerosols; Sect. 4 gives a qualitative and quantitative evaluation of the enhancement of the hygroscopic properties by coating with soluble material. A summary and some conclusions are given in Sect. 5.

## 2 Observations and model description

### 2.1 Observations

The observations were acquired during an intensive campaign combining airborne, in situ and remote sensing measurements named EUCAARI-IMPACT (where IMPACT stands for Intensive Observation Period at Cabauw Tower), which took place in May 2008. During this campaign, airborne measurements were made using the French ATR-42 aircraft. The calibration of the devices onboard the ATR-42 aircraft during the EUCAARI-IMPACT campaign and the evaluation of their performance are discussed in detail by Crumeyrolle et al. (2013) and are only briefly described here. The aerosol instrumentation sampled the particles via the ATR-42 community aerosol inlet (CAI) (Crumeyrolle et al., 2013). The CAI was designed for the ATR to allow

isokinetic and isoaxial sampling relative to the incoming air stream. This inlet has a 50 % sampling efficiency for particles with diameters around 5  $\mu\text{m}$  (Crumeyrolle et al., 2008, 2010, 2013; McNaughton et al., 2007). The total ambient aerosol concentrations were measured by a condensation particle counter (CPC, TSI model 3010) aboard the ATR-42 aircraft every 1 s. The 50 % detection efficiency of the TSI 3010 CPC applies to particles of diameter larger than 10 nm and its relative uncertainty is about 5 % (Mertes et al., 1995). The cloud condensation nuclei counter (CCNC, DMT model no. CCN-100) onboard the ATR-42 aircraft was a continuous-flow streamwise thermal gradient CCN counter (Crumeyrolle et al., 2013). The design and operating principles of the instrument are based on the work of Roberts and Nenes (2005). The supersaturation was set at 0.2–0.4 % during all the research flights. The chemical composition and mass concentration of the aerosol were analyzed through the use of a time-of-flight aerosol mass spectrometer (C-ToF-AMS, Middelbrook et al., 2012; Canagaratna et al., 2007) aboard the ATR-42 aircraft. The AMS provided information on the mass concentration of particulate organic matter (POM), nitrate, ammonium and sulfate. It should also be noted that the upper 50 % cut-off-diameter of the onboard AMS is about 500 nm (Crumeyrolle et al., 2013). As reported by Ansmann et al. (2011) airborne multiwavelength backscatter lidar has proved to be a powerful technique for detecting dust plumes and their properties. In order to analyze the optical properties of the dust plume, the LEANDRE new generation (LNG) lidar was used in its backscatter version. The LNG airborne backscatter lidar is currently used for aerosol characterization (de Villiers et al., 2010; Pelon et al., 2002; Schepanski et al., 2013). During the EUCAARI-IMPACT campaign, the system was operated in backscatter mode with three elastic channels at 1064, 532 and 355 nm, and depolarization ratio at 355 nm. Energies of 10 and 50 mJ were emitted at the upper two wavelengths, respectively, at 20 Hz repetition rate with a full angle divergence of the laser of 4 mrad at 532 nm and 6.5 mrad at 1064 nm. The profiles of atmospheric extinction coefficient at 532 nm were retrieved using a standard lidar inversion technique (Cuesta et al., 2008; Klett, 1985; Fernald, 1984), after normalization to molecular scattering (see de Villiers et al., 2010, for more information).

During the EUCAARI-IMPACT campaign, the instruments of the Cabauw Experimental Site for Atmospheric Research (CESAR, 51.97° N, 4.93° E) were deployed. This site was selected as a supersite to quantify the regional aerosol properties, including aerosol formation, transformation, transport and deposition (Kulmala et al., 2009). We used data recorded from the DMT-CCNC (model no CCN-100, Roberts and Nenes, 2005) which operated continuously during this intensive observational period with a supersaturation in the range of 0.1 to 0.7 %. We also used the observations from the C-ToF-AMS and the multi angle absorption photometer (MAAP 5012, Petzold and Schronlinner, 2004) in order to describe the chemical composition

and mass concentration of the aerosol over Cabauw. In order to evaluate the temporal and spatial evolution of the pollution aerosol over Europe, the BC mass concentration recorded by other European ground sites with a MAAP 5012 were also used. The ground sites selected were the European Supersites for Atmospheric Aerosol Research (EU-SAAR) sites at Monte Cimone (44.11° N, 10.42° E), Puy-de-Dôme (45.46° N, 2.57° E) and Hohenpeißenberg (47.80° N, 11.01° E).

The Cloud-Aerosol Lidar and Infrared Pathfinder Satellite Observation (CALIPSO) products were used to analyze the dust outbreak. The Cloud-Aerosol Lidar with Orthogonal Polarization (CALIOP) is a two-wavelength polarization-sensitive lidar on board the CALIPSO satellite mission. An overview of the CALIPSO mission is given by Winker et al. (2010). The CALIPSO products used in this work were selected at level 1 because the level 2 products were unavailable for data acquired prior to 14 September 2008. The main level 1 CALIPSO products are the total attenuated backscatter profiles with a vertical and horizontal resolution of 30 and 1 m respectively below 8.2 km (Winker et al., 2009). The technical details of these data sets are described in the CALIOP algorithm theoretical basis document (<http://eosweb.larc.nasa.gov>).

## 2.2 Back trajectory model: LACYTRAJ

LACYTRAJ is a kinematic back trajectory code using the ECMWF wind field developed at the Laboratoire de l'Atmosphère et des Cyclones (LACy, France) (Baray et al., 2012; Clain et al., 2010; Duflot et al., 2010). This code was used to determine the sources of the air masses arriving above Cabauw. Each air parcel was advected using a bilinear interpolation for horizontal wind fields and time, and a log-linear interpolation for vertical wind field. This operation is performed with a time step defined by the user: 10 min in this work, over a six-day period. The sensitivity and comparative study carried out by Clain et al. (2010) with LACYTRAJ and other models such as FLEXPART highlights the capability of LACYTRAJ for back trajectory analysis. Details on this code can be found in Clain et al. (2010).

## 2.3 Meso-NH model

The simulations in this study were performed with the meso-scale, non-hydrostatic atmospheric model Meso-NH. This model was developed jointly by the Centre National de la Recherche Meteorologique (CNRM, France) and the Laboratoire d'Aerologie (LA, CNRS) (Lafore et al., 1998). Meso-NH allows simulations from small scale (LES type) to synoptic scale (horizontal resolution ranging from a few meters to several tens of kilometers). Furthermore, the two-way interactive grid-nesting method allows the model to be run simultaneously on several domains with the same vertical levels but with different horizontal resolution. Meso-NH contains

various sets of parameterizations such as cloud microphysics (Cohard et al., 2000; Cohard and Pinty, 2000), turbulence (Bougeault and Lacarrere, 1989), lightning processes (Barthe et al., 2005), gas-phase chemistry (Tulet et al., 2003; Suhre et al., 1998), aerosol chemistry (Tulet et al., 2005, 2006) and dust aerosol (Tulet et al., 2010; Grini et al., 2006). Natural land surfaces are described by interactions treated in the Interactions Soil-Biosphere-Atmosphere model (ISBA) (Noihran and Mahfouf, 1996).

### 2.3.1 Aerosol parameterization

In addition to solving the prognostic meteorological variables, Meso-NH computes the gaseous chemistry evolution and solves the aerosol equilibrium at each grid point and at each time step (Tulet et al., 2003). This study uses the Reduced Lumped Atmospheric Chemical Scheme 2 (RELACS2) chemical reaction scheme, which includes 82 species (Tulet et al., 2006). RELACS2 is based on the Caltech Atmospheric Chemistry Mechanism (CACM) scheme developed by Griffin et al. (2002). It is coupled with the aerosol scheme ORILAM (Organic Inorganic Log-normal Aerosol Model) (Tulet et al., 2005, 2006) online. The ability of ORILAM to simulate aerosol processes, such as nucleation, coagulation, condensation, sedimentation and dry deposition, has been highlighted in several recent studies (Schepanski et al., 2013; Bègue et al., 2012; Aouizerats et al., 2012, 2011; Chaboureau et al., 2011). A detailed description of ORILAM is given by Tulet et al. (2005), and is briefly presented here. ORILAM uses a three log-normal parameterization. Thus, ORILAM assumes that the aerosol size distribution consists of log-normal modes that can be described by the 0th, 3rd and 6th moment of the distribution (Tulet et al., 2005, 2006). For diagnostic purposes, the moments can be transformed into number concentration, number median diameter and geometric standard deviation. In this study, the 6th moment was kept constant, which implies that the dispersion of each aerosol mode was kept constant during the simulation. ORILAM takes a range of aerosol species considered as internally mixed, such as black carbon (BC), primary organic aerosol (OC), nitrate, sulfate, ammonium and ten classes of secondary organic aerosols (SOA<sub>1</sub>, ..., SOA<sub>10</sub>) defined by Griffin et al. (2002). Moreover, ORILAM also considers the dust and sea salt aerosol as externally mixed. However, in the framework of this study, the dust was introduced into the other aerosol species as internally mixed. The dust fluxes were calculated from wind friction speed using the dust entrainment and deposition (DEAD) model (Zender et al., 2003), which is implemented as a component of Meso-NH (Mokhtari et al., 2012; Grini et al., 2006). The physical basis of the model is taken from Marticorena and Bergametti (1995), in which dust fluxes are calculated as a function of saltation and sandblasting processes. The initial dust size distribution contains three log-normal modes with median radii of 0.039, 0.32 and 2.5 µm and standard deviation

tion of 1.75, 1.76 and 1.70 respectively. ORILAM drives both the dynamical processes and the thermodynamical equilibrium between gases and particles along the Model to Predict the Multiphase Partitioning for Organics (MPMPO) scheme for organic species (Griffin et al., 2005) and the Equilibrium Simplified Aerosol Module (EQSAM, Metzger et al., 2002) for inorganic species in order to solve the condensation and nucleation processes. The aerosol radiative properties (extinction coefficient, asymmetry factor and single scattering albedo) are computed within ORILAM. They are then processed as inputs by the ECMWF radiation scheme implemented and coupled online with Meso-NH and AROME (Aouizerats et al., 2010; Tulet et al., 2008).

Aerosol-cloud interaction including impact-scavenging is determined according to a kinetic approach to calculate the aerosol mass transfer in cloud and rain droplets as defined by Tost et al. (2006). The scavenging by raindrops depends mainly on Brownian motion, interception and inertial impaction as described by Slinn (1979). The collection efficiency obtained from the scavenging schemes used in this study is calculated by taking these three types of collection into account. For the present study, we used an explicit and an implicit scavenging scheme (Bègue et al., 2012; Tulet et al., 2010). The implicit aerosol scavenging is parameterized following the mass flux calculated from the deep and shallow convection parameterization (Bechtold et al., 2001) based upon the Kain and Fritsch (1993) mass flux scheme. Deep and shallow convective drafts exchange mass horizontally with their environment through detrainment of cloudy air and entrainment of cloud-free air. Subgrid-scale entrainment and detrainment fluxes are diagnosed in terms of grid-scale thermodynamic and dynamic variables (Bechtold et al., 2000). The ICE3 microphysics scheme (Pinty and Jabouille, 1998) is used to resolve the wet deposition parameterization for the explicit scheme (Tulet et al., 2010).

### 2.3.2 CCN activation scheme

The supersaturation and the number of activated CCN were estimated from the aerosol chemical composition and size distribution computed by ORILAM. The CCN activation scheme used in this study is based on the parameterization proposed by Abdul-Razzak and Ghan (2000, 2004), which has been widely included in many models as reported by Ghan et al. (2011). The ability of this scheme to diagnose the number of activated CCN has been highlighted in several recent studies (Ghan et al., 2013; Bangert et al., 2011; Song and Zhang et al., 2011). The physical basis of the CCN activation scheme is derived from Köhler's theory (1936), in which water vapor condenses on inorganic salt particles to form water droplets. The Köhler theory is used to relate the aerosol size distribution and chemical composition to the number of activated CCN as a function of supersaturation (Abdul-Razzak and Ghan, 2000). The maximum supersaturation is calculated from the aerosol properties and the updraft veloc-

ity. The scheme thus takes the effect of aerosol composition (Raoult term) and the surface tension effect (Kelvin term) on hygroscopicity into account. The Raoult term was parameterized by assuming additive behavior of the inorganic salt and the organic surfactant when these aerosol species were internally mixed (Abdul-Razzak and Ghan, 2000; Shulman et al., 1996). Following Abdul-Razzak and Ghan (2004), the Kelvin term was parameterized from Szyskowski's empirical equation (Szyskowski, 1908).

### 2.3.3 Simulation configuration

The simulation started at 00:00 UTC on 25 May 2008 and ended at 00:00 UTC on 1 June 2008. The study domain, covering the EUCAARI campaign area and a large part of the northern Africa, extended between latitudes 15.1 and 68.7° N and longitudes 14.9° W and 23.1° E, with a grid spacing of 25 km. This domain allowed a large-scale view of the dust plume towards northwestern Europe. The vertical grid spacing consisted of 60 stretched vertical levels reaching an altitude of 30 km. Initialization and boundary conditions for the large domain were provided by the global chemical transport model MOCAGE (Dufour et al., 2004) for the chemical gaseous part and the ECMWF operational analysis for atmospheric dynamics. The simulations performed included the implicit and explicit aerosol scavenging schemes. "Off-line" sensitivity analyses of CCN activation were performed for different supersaturations in order to assess the contribution of the aged dust to the CCN concentration measured over Cabauw.

In order to obtain a correct representation of the gas-phase chemistry and the aerosol particle concentration, an emission inventory of gases and particles was used. The emission inventory was developed by the Netherlands Organization for Applied Scientific Research (TNO) from measurements made during the MEGAPOLI (Megacities: emission, urban, regional and global atmospheric pollution and climate effect and integrated tools for assessment and mitigation) campaign (Baklanov et al., 2008). This emission inventory includes an hourly-based description for the species: BC, OC, CO, SO<sub>2</sub>, NH<sub>3</sub>, NO<sub>x</sub> and volatile organic compounds (VOCs), emitted during the study period. The emissions are located in a domain extending between latitudes 34.2 and 54.9° N and longitudes 9.9° W and 19.9° E. The biogenic emissions were initialized from the MEGAN (Model of emission of gases and aerosols from nature) inventory with a resolution of 0.5°.

### 3 Interaction of an intense dust plume with pollution aerosol during its transport over northwestern Europe

#### 3.1 Transport of intense plume over northwestern Europe

The back trajectory calculated with LACYTRAJ for the period of 25–30 May highlights the presence of an air mass over Cabauw on 30 May which appears to come from Northern Sahara, on 25 and 26 May (Fig. 1). Source regions at latitudes close to 22° N (1° W) and 33° N (6° E) could be respectively identified from CALIPSO observations (not shown). This is in agreement with Crumeyrolle et al. (2013), who used FLEXPART to show the presence of an air mass in the boundary layer (BL) and the lower free troposphere (LFT) at Cabauw, which originated in northern Africa. The back trajectory analysis also revealed that the Saharan air mass left Africa at the end of 26 May and reached Europe two days later. On 30 May, the Saharan air mass continued its spread to Cabauw via eastern France and Switzerland (Fig. 1). It should also be noted that the chronology obtained from the back trajectory analysis is consistent with that reported by Bègue et al. (2012) from satellite observations.

An overview of the dust event at 01:00 UTC on 28 May and 02:00 UTC on 29 May 2008 is given in Fig. 1a and b through the dust burden and wind fields simulated by Meso-NH. The transport of the dust plume over northwestern Europe took place in a meteorological situation disturbed by strong convective activity associated with the passage of a frontal system over Europe (Hamburger et al., 2011). The wind flow at 700 hPa revealed a strong flow from northern Africa moving northeast towards the Mediterranean Sea (Fig. 1a and b). Over the Mediterranean basin, the Saharan air mass was embedded in a flow moving towards the northwest and transported toward the shores of the Baltic Sea (Fig. 1a and b). According to Bègue et al. (2012), this flow was produced by a trough extending along the European and African coast and an area of high-pressure located over central Europe. The transport of the dust plume over northwestern Europe was modulated by the strength and position of the high pressure associated with the frontal system.

On 28 May 2008 at 01:00 UTC, the model results show a belt of high dust burden extending in a large area from central Algeria to Switzerland passing through northwestern Italy (Fig. 1a). According to the model, inside this area, the values exceed  $8 \text{ g m}^{-2}$ , especially over northwestern Libya and Sardinia where values of 10 and  $9.5 \text{ g m}^{-2}$ , respectively, are simulated. On 29 May, the belt of high dust burden has disappeared (Fig. 1b). The simulated dust burden has decreased by more than half in the Italian and Mediterranean regions (values do not exceed  $4 \text{ g m}^{-2}$ ). This considerable decrease is the consequence of the interaction between the dust plume and the convective activity. Bègue et al. (2012) have shown that precipitations scavenged the majority of dust over the

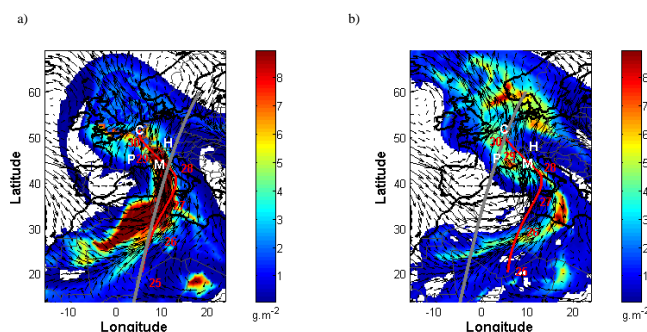


**Figure 1.** Dust load (shading,  $\text{g m}^{-2}$ ) and 700 hPa wind (vectors) simulated by Meso-NH at 12:00 UTC on (a) 28 May and (b) 29 May 2008. Nighttime CALIPSO overpasses are indicated by the gray line. Six-day backward trajectories calculated during the 25–30 May 2008 period are indicated by the red line. The locations of the Cabauw, Puy de Dôme, Hohenpeißenberg and Mont Cimone sites are indicated by C, P, H and M respectively.

Mediterranean and European regions. In particular, this interaction led to high precipitation scavenging efficiency for the dust coarse mode. In contrast, the dust burden increased over Scandinavia, with the maximum value (around  $7 \text{ g m}^{-2}$ ) simulated over Norway (Fig. 1b). Overall, there is fairly good agreement between the simulations presented here and those reported in the literature (Bangert et al., 2012; Pappalardo et al., 2010).

From the CALIOP observations (Fig. 2a), the vertical structure of aerosols can be assessed over a long range, here from northern Africa to central Europe at 01:00 UTC on 28 May (see the CALIPSO track in Fig. 1a). As checked using the feature mask of CALIPSO products (not shown), observed total attenuated backscatter (ATB) signals ranging from  $1 \times 10^{-3}$  to  $5 \times 10^{-3} \text{ km}^{-1} \text{ sr}^{-1}$  (corresponding to scattering ratio up to 3) were due to the Saharan plume. This is confirmed by an average particle depolarization ratio equal to 30 % (Fig. 4). On the 28 May, over the sources in the region (24.6° N, 7.7° E–36.5° N, 10.9° E), the dust plume stretched from the surface to 6 km a.s.l. (Fig. 2a). The major dust plume was transported towards the Mediterranean and European regions between 2 and 5 km a.s.l. This also confirms by an average particle depolarization ratio equal to 30 % (Fig. 4). It is seen in CALIPSO lidar observations that the particulate depolarization ratio is about 20–25 % from 46 to 48° N and altitudes between 2 and 5 km (Fig. 4). This confirms the possibility of mixing between the dust plume and anthropogenic aerosol over Europe. Due to the reconstructed trajectory, it can be assumed that the dust plume interacted with the foothills of the African continent during its transport. The elevation of the dust plume height when it came out of the African continent was very likely due to the interaction between the plume and the foothills of northern part of the Hoggar and the synoptical atmospheric forcing resulting in the north-easterly flow (Fig. 2a). The Meso-NH sim-



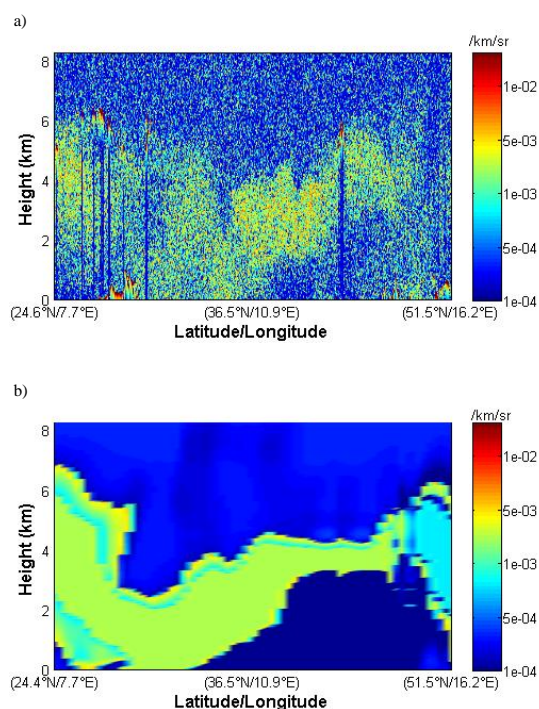


**Figure 2.** The total attenuated backscatter ( $\text{km}^{-1} \text{sr}^{-1}$ ) at 532 nm from (a) the CALIPSO product and (b) the Meso-NH simulation for the overpass at 01:22–01:27 UTC on 28 May 2008. The CALIPSO overpass on 28 May 2008 is indicated by the gray line in Fig. 1a.

ulation reproduced the features of the vertical structure and the observed ATB signals fairly well (Fig. 2b). However, the simulated plume over the Mediterranean and European regions was thinner (between 2 and 4 km, see Fig. 2b) than the observed plume. As already discussed, Bègue et al. (2012) showed the interaction between the dust plume and the convective activity over Europe, particularly on 29 May, when the convective activity was the most intense. From CALIOP observations (Fig. 3a), the vertical structure of clouds and aerosols can be assessed over a long range, here from the Mediterranean to northern Europe at 02:00 UTC on 29 May (see the CALIPSO track in Fig. 1b). The observed ATB signals larger than  $10^{-2} \text{ km}^{-1} \text{sr}^{-1}$  were due to clouds. The high clouds were particularly observed over northern France ( $48.2^\circ \text{N}$ ,  $4.0^\circ \text{E}$ ) but also over Massif Central ( $45^\circ \text{N}$ ,  $2^\circ \text{E}$ ). Attenuation below the dense high clouds prevented the observation of most of the structures below. Midlevel clouds were observed from Belgium to Scandinavia (Fig. 3a). The simultaneous presence of clouds and dust were particularly observed over the Netherlands and Scandinavia. The interactions between dust and clouds appears to take place between 2 and 5 km a.s.l. (Fig. 3a). It can be noted that the presence of dust on 29 May at latitudes higher than  $50^\circ \text{N}$  and altitudes below 4 km is confirmed by the particulate depolarization ratio equal to 30 % (Fig. 4).

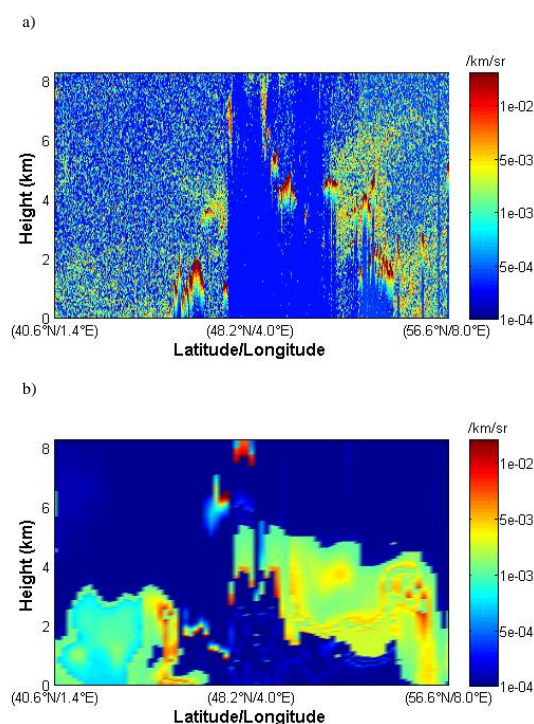


**Figure 3.** The total attenuated backscatter ( $\text{km}^{-1} \text{sr}^{-1}$ ) at 532 nm from (a) the CALIPSO product and (b) the Meso-NH simulation for the overpass at 02:00–02:06 UTC on 29 May 2008. The CALIPSO overpass on 29 May 2008 is indicated by the gray line in Fig. 1b.

The features of the vertical structure of the dust plume were acceptably reproduced by Meso-NH whereas the vertical structures of clouds were insufficiently reproduced (Fig. 3b). The main reason for this discrepancy can be attributed to the fact that a subgrid resolution of 25 km is not sufficient to reproduce the convective activity properly. Overall, Meso-NH reproduced the dust transport toward north-western Europe acceptably well.

### 3.2 Temporal and spatial evolution of the anthropogenic aerosol

The BC mass concentration and the wind field at the surface simulated by Meso-NH on 28 and 29 May are depicted in Fig. 5a and b respectively. On 28 May, the high BC mass concentrations are mainly located in northern and central Europe (Fig. 5a). Model results show a large area of high BC mass concentration extending from the English Channel to Norway passing along the shore of the Netherlands and Denmark. Within this area, the values exceed  $1.9 \mu\text{g m}^{-3}$ , particularly over the English Channel and the coast of the Netherlands, where values of 2.5 and  $2.2 \mu\text{g m}^{-3}$  are simulated respectively. A second belt of high BC mass concentration ( $1.9$  to  $2.2 \mu\text{g m}^{-3}$ ) simulated on 28 May extends in a large area from southeastern France to the Netherlands (Fig. 5a). On 29 May, the second belt of high BC mass concentration lo-



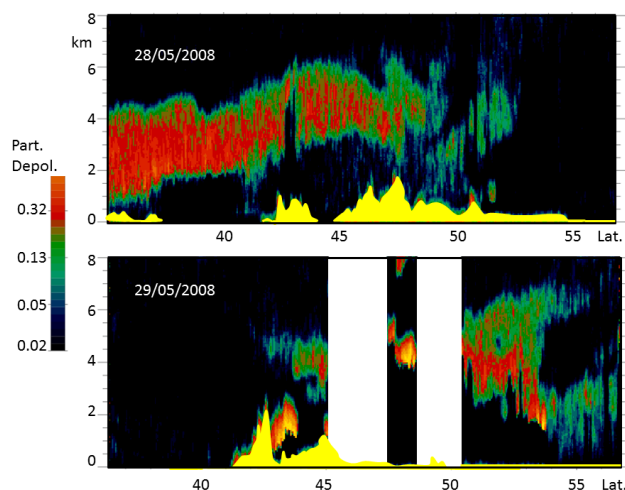


**Figure 4.** CALIPSO particle depolarization at 532 nm for the overpass at 01:22–01:27 UTC on 28 May 2008 (top) and the overpass at 02:00–02:06 UTC on 29 May 2008 (bottom). The CALIPSO overpasses on 28 and 29 May 2008 are indicated by the gray line in Fig. 1a and b respectively. The topography is depicted in yellow. The data noised by the high clouds were removed to the picture (blank area).

cated over Central Europe has disappeared and, in the Northern region, the simulated BC mass concentration has decreased by more than half (value not exceeding  $1.1 \mu\text{g m}^{-3}$ ) (Fig. 5b).

The simulated sulfate concentrations and the wind field at the surface on 28 and 29 May are shown in Fig. 5c and d respectively. On 28 May, areas with high sulfate concentrations are located over northern Europe and Corsica. Over northern Europe, a wide area of high sulfate concentrations (maximum value of  $6.2 \mu\text{g m}^{-3}$ ) extending from Norway to the Netherlands is simulated (Fig. 5c). On 29 May, the high sulfate concentration areas are mainly situated over northern and central Europe (Fig. 5d) with a local maximum over the English Channel where the maximum concentration of sulfate ( $6.5 \mu\text{g m}^{-3}$ ) is simulated. Overall, the simulation results show that the concentrations of anthropogenic aerosol are particularly high over northern Europe. This analysis of the spatial distribution of the anthropogenic aerosol is in agreement with the work of Hamburger et al. (2011), who have shown that the synoptic situation during May 2008 led to an accumulation of aerosol inside the planetary boundary layer (PBL), and particularly over northern Europe. Furthermore, they found that the maximum aerosol concentration was observed within the PBL above Cabauw.

The observed BC mass concentration is compared with the concentrations simulated by Meso-NH in Fig. 6. The Mont Cimone station is located in the northwestern corner of Italy, which is the site with the lowest BC mass concentration among the stations selected. The observed BC mass concentration ranged from  $0.2$  to  $0.9 \mu\text{g m}^{-3}$  with a maxi-

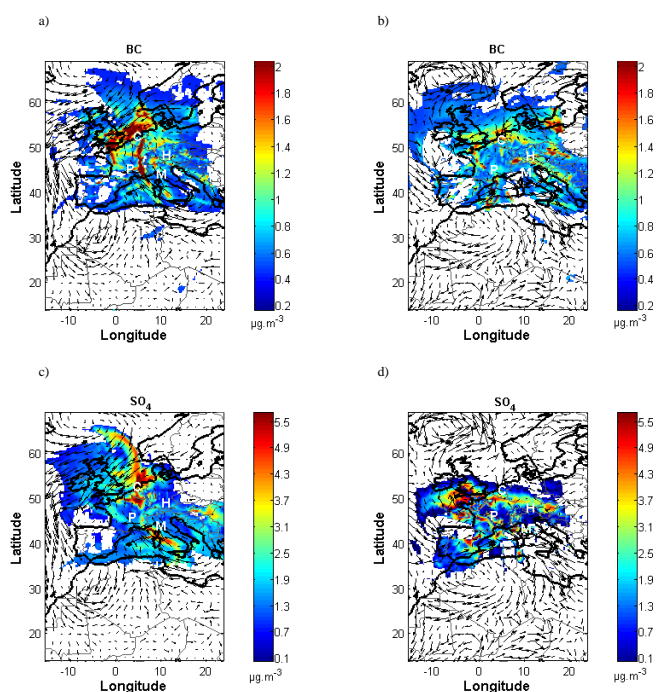


**Figure 5.** BC (a, b) and sulfate (c, d) mass concentration simulated by Meso-NH at 12:00 UTC on 28 May (a, c) and 29 May (b, d) 2008. The locations of the Cabauw, Puy de Dôme, Hohenpeißenberg and Mont Cimone sites are indicated by C, P, H and M respectively.

um value occurring on 25 May. After 25 May, BC concentrations quickly decreased to under  $0.5 \mu\text{g m}^{-3}$  until 31 May (Fig. 6a). This temporal evolution appears to be correctly simulated. The BC mass concentration observed over Puy-de-Dôme ranged from  $0.3$  to  $1.2 \mu\text{g m}^{-3}$  (Fig. 6b). We note that the BC mass concentration evolution over Puy-de-Dôme follows a daily cycle with a maximum observed at midday and a minimum observed during the night. Over the Hohenpeißenberg station, the observed BC mass concentration ranged from  $0.3$  to  $1.8 \mu\text{g m}^{-3}$  with the maximum occurring on 25 May (Fig. 6c). The BC mass concentration increased to  $1.8 \mu\text{g m}^{-3}$  on 25 May and slowly decreased afterwards to  $0.9 \mu\text{g m}^{-3}$  until 31 May, which is in agreement with the simulation results. However, we note the presence of a time shift of 2 days between the maximum value observed (25 May) and simulated (27 May). It can be noted for the three stations mentioned above that the BC mass concentration tends to decrease during the study period. The Cabauw station, which is located in a rural area in the central part of the Netherlands, is the site with the highest BC mass concentration in comparison with the three others. In contrast to what happens at the other stations, the BC mass concentration observed here tends to increase during the study period with values ranging from  $0.5$  to  $2.5 \mu\text{g m}^{-3}$  (Fig. 6d). In spite of an underestimation ( $0.3 \mu\text{g m}^{-3}$  on average), the temporal evolution of

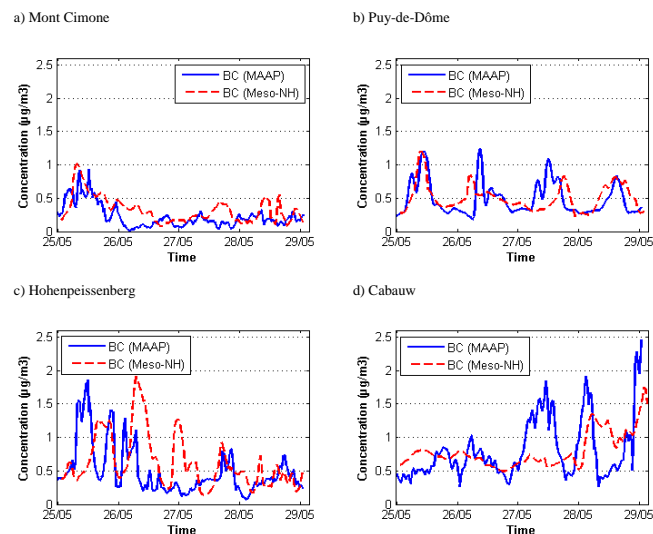


**Figure 6.** Evolution of the BC mass concentration ( $\mu\text{g m}^{-3}$ ) simulated (red dashed line) and measured (blue solid line) between 25 and 29 May 2008.

the BC mass concentration over Cabauw is fairly well reproduced by Meso-NH.

The discrepancies between Meso-NH and the observations may be attributable to several sources. First, a possible source of error can come from the fact that Meso-NH is an atmospheric forecasting model and drives the evolution of its meteorological fields itself. As such, it makes its own forecast and, as for all atmospheric models, a drift can appear in the forecast and increase as the simulation advances away from the initial conditions. Another possible explanation for the differences can come from the fact that the aerosol concentrations are calculated for grid cells with 25 km horizontal resolution. However, the overall temporal evolution of BC mass concentrations simulated by Meso-NH is in acceptable agreement with the observations. Moreover, both the observations and the simulations show that the highest anthropogenic aerosol concentrations are mainly located over northern Europe.

### 3.3 Mixing of the dust plume with the European pollution aerosol

In order to highlight a possible interaction between the dust plume and European pollution, a vertical cross section of the dust and anthropogenic aerosol mass concentrations between the surface and 6 km a.s.l. along the trajectory obtained from LACYTRAJ between 28 and 30 May (Fig. 1) was drawn from the concentrations calculated by Meso-NH and is shown Fig. 7. During 28 May, a dust concentration of  $500 \mu\text{g m}^{-3}$  spread along the western coast of Italy towards Switzerland at between 1 and 3.8 km a.s.l. Given that the plume continued its propagation along the eastern coast of France, the diminution of the vertical coverage of

the dust plume (2–3 km a.s.l.) and the dust concentration ( $400 \mu\text{g m}^{-3}$ ) simulated on 29 May can be explained by the interaction between the plume and the foothills of the Vosges mountains. On 30 May, the dust plume moved from Belgium to the Netherlands, where it separated into two layers. These two main dust layers were separated by a region of weak concentration (not greater than  $250 \mu\text{g m}^{-3}$ ). The first dust layer was situated between 2 and 4.2 km a.s.l. with a dust concentration range of 370 to  $400 \mu\text{g m}^{-3}$ . In contrast, the second layer was located near the surface and was thinner than the first (0.8–1.5 km a.s.l.) with dust concentration ranging from 320 to  $370 \mu\text{g m}^{-3}$ . Bègue et al. (2012) described this structure in two layers as resulting from the interaction of the dust plume with the convective activity. The present simulations show that this structure in two layers can be also due to the interaction of the plume with the foothills of the Vosges mountains during its transport toward the Netherlands.

An overview of the simulated carbonaceous (BC + OC) and inorganic salts mass concentration along the dust plume trajectory during the period of 28–30 May are given in Fig. 7. The simulated carbonaceous mass concentration reaches  $7 \mu\text{g m}^{-3}$ , with the maximum located at 1.5 km a.s.l. The vertical coverage of the carbonaceous component extends from surface up to 2.5 km a.s.l. on 30 May (see Fig. 7). Thus, we note the interaction of the carbonaceous component with the lower dust plume on 28 May during its spread towards Switzerland (Fig. 7). Moreover, this layer also interacted with the organic component on 30 May over Belgium and the Netherlands (Fig. 7). The simulated inorganic salts mass concentration reached  $40 \mu\text{g m}^{-3}$  with the maximum located near the surface over Italy. The vertical coverage of the inorganic salts was lower than the carbonaceous component, in particular over central Europe where, on 28–29 May, the vertical extent of the inorganic salts extended from the surface to 1 km a.s.l. On 30 May, the vertical extension of the inorganic salts increased and ranged up to 2 km a.s.l. over Belgium and the Netherlands (Fig. 7). The simulations thus show that the lower dust layer has most probably been able to interact with the organic salts mainly over Belgium and the Netherlands. It can also be noted that the mixing occurred essentially with the dust from the first layer. Although the mixing between the dust and the inorganic salts occurred mainly over Belgium and the Netherlands, it can be observed that the amount of inorganic salt mixed with the dust was greater than the carbonaceous component. It is worth noting that the species simulated above the PBL are the residual pollution produced the previous days and coming from the southeast of France, as it was shown by Bègue et al. (2012). The above results clearly show the mixing between the dust plume and the anthropogenic aerosol, particularly over the northern part of Europe.

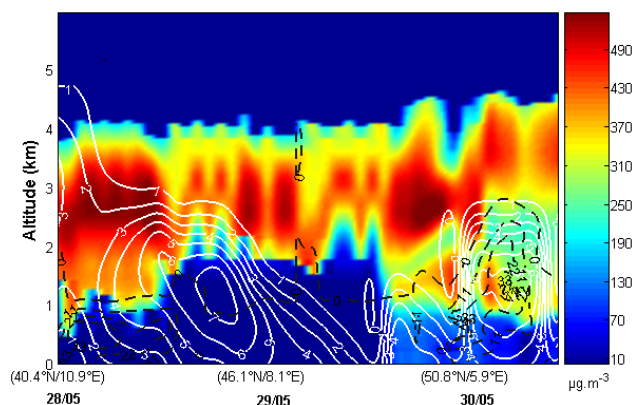


**Figure 7.** Vertical cross section of dust mass concentration (shading) with carbonaceous component mass concentration (white line, BC and OC) and inorganic salts mass concentration (black dashed line) following the dust plume trajectory over Europe between (40.4° N, 10.9° E) and (56.6° N, 8.0° E) obtained from the simulation.

## 4 Enhancement of the hygroscopic capacity of the dust plume over the Netherlands

### 4.1 Chemical composition of the aerosol

We propose now to quantify the impact of this mixing on the hygroscopic and CCN properties of the dust plume. Inside this section, the consequence of this mixing over the Netherlands on the dust hygroscopic properties will be discussed in detail. The extinction coefficient obtained from the LNG on board the ATR-42 aircraft on 30 May from 13:11 to 14:01 UTC over the Netherlands is shown in Fig. 8. It was measured over a domain between latitudes 52.57 and 51.88° N and longitudes 6.34 and 4.99° E. The vertical cross section obtained with LNG observations reveals that the extinction coefficient ranges from 0.01 to 5 km<sup>-1</sup> between 0.8 to 3 km a.s.l. (Fig. 8a). As shown previously with the CALIPSO product (Sect. 3.1), northern Europe was affected by the presence of high and mid-level clouds during this period. The observed extinction coefficients higher than 0.4 km<sup>-1</sup> were hence due to clouds. It is seen in CALIPSO lidar observations that the particulate depolarization ratio is about 15 % at latitudes higher than 53° N and altitudes below 3 km outside clouds on 28 and 29 May 2008 (Fig. 4). Over the Netherlands, the LNG observations show a permanent stratocumulus cloud layer at 0.7 km a.s.l. (Fig. 8a). In these lidar observations, we also note the presence of clouds between 2.2 and 2.5 km a.s.l. embedded in a medium scattering and depolarizing layer. In this elevated layer, outside the high backscattering cloud regions (near 13:30 UTC for example, see Fig. 8a), the scattering ratio at 532 nm is close to 4 between 2.3 and 2.5 km but depolarization is determined to be smaller than 15 % following de Villiers et al. (2010). These clouds layers are more heterogeneous than those observed at

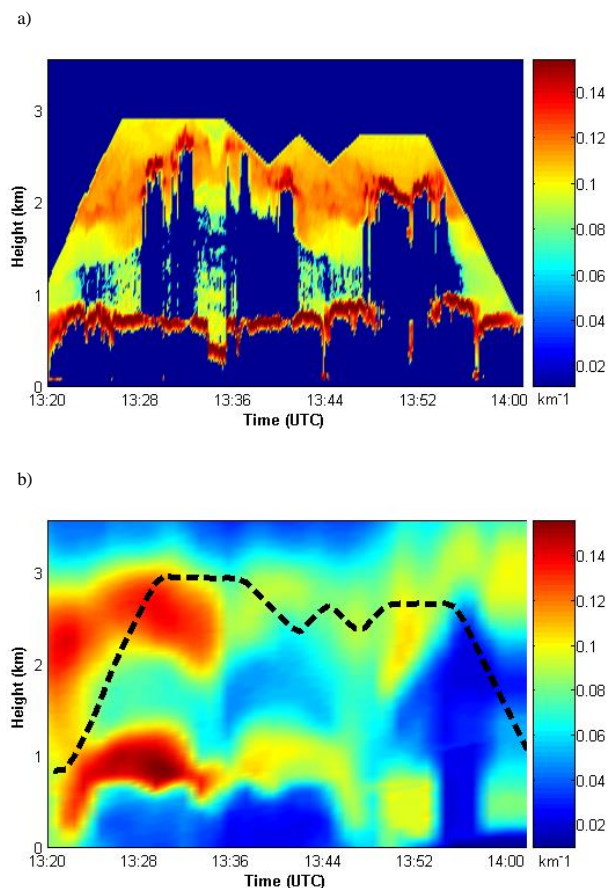


**Figure 8.** Vertical cross section of extinction coefficient (km<sup>-1</sup>) (a) measured by LEANDRE and (b) simulated by Meso-NH over the Netherlands between (52.57° N, 6.34° E) and (51.88° N, 4.99° E) on 30 May 2008. The black line indicates the height of the aircraft. All the blue areas in the upper plot (LEANDRE observation) are areas without data.

800 m above the surface. The aerosol air mass indeed appears to be structured in two main layers separated by a region of weak extinction coefficient (from 0 to 0.06 km<sup>-1</sup>). Furthermore the analysis of the LNG data reveals that the particle color ratio is smaller than 0.2 in the region where the extinction exceeds 0.11 km<sup>-1</sup>. This corresponds to a backscatter Angström coefficient larger than 2, which is indicative of a strong contribution of small size particles (Catrall et al., 2005).

It should be noted that this structure, obtained from LNG observations, is quite similar to the structure of the simulated dust plume over the Netherlands. The first aerosol layer is observed between 1.6 and 2.8 km a.s.l. with the extinction maximum (0.16 km<sup>-1</sup>) located between 1.8 and 2.5 km high. The second layer is located between 0.6 and 0.7 km a.s.l. and is separated into two parts by a region of low values (less than 0.01 km<sup>-1</sup>). We note that this aerosol layer is continuously masked by the cloud layer (Fig. 8a). To understand this verti-



cal structure of atmospheric aerosol, the remote sensing measurements were reproduced by the Meso-NH model for comparison (Fig. 8b). The simulated extinction coefficient compared relatively well with the observed one. The contribution of the dust to extinction was analyzed over this region from the Meso-NH simulation. These simulation results reveal that 90 % of extinction is due to dust. Bègue et al. (2012) demonstrated that optical parameters (scattering, extinction, single scattering albedo) measured during this flight from 13:50 to 14:05 UTC were mainly due to the dust accumulation mode. This is also confirmed by the color ratio close to 0.5 as derived from the lidar measurements at 532 and 1064 nm, normalization the ratio at 1 on the stratocumulus cloud. This predominance of the dust accumulation mode is consistent with the in situ measurements from ATR-42 (Crume rolle et al., 2013). Based on the SMPS measurements recorded onboard the ATR-42, they showed an enhancement of the accumulation mode particle number concentration in both BL and LFT. They also showed an enhancement of the total mass concentration in the intermediate layer (1–3 km), suggesting efficient long-range transport of aerosol particles.

The mass concentration of inorganic salts (nitrate, sulfate, ammonium) and OC obtained with the AMS (type: c-TOF) onboard the ATR-42 during the same flight is shown in Fig. 9. Because of the presence of clouds, data were not recorded everywhere during the flight. The  $\text{NH}_4$  mass concentration increased and reached its maximum value ( $5.3 \mu\text{g m}^{-3}$ ) at 0.8 km a.s.l. from 13:11 to 13:25 UTC, and decreased afterwards to  $0.2 \mu\text{g m}^{-3}$  between 1 and 2.8 km a.s.l., before oscillating between 0.1 to  $5 \mu\text{g m}^{-3}$  until the end of the flight (Fig. 9a). The evolution of sulfate and OC looks similar to the evolution of the ammonium mass concentration. Thus, the sulfate and OC mass concentrations reached their maximum values (10 and  $7 \mu\text{g m}^{-3}$  respectively) near the surface, and decreased together thereafter to  $0.1 \mu\text{g m}^{-3}$  between 1 and 2.8 km a.s.l., before oscillating between 0.1 and  $5 \mu\text{g m}^{-3}$  for the sulfate, and between 0.1 and  $2 \mu\text{g m}^{-3}$  for the OC until the end of the flight (Fig. 9b and c). The nitrate mass concentration increased to  $5 \mu\text{g m}^{-3}$  at 0.8 km a.s.l., and quickly decreased to  $0.1 \mu\text{g m}^{-3}$  between 1 and 2.8 km a.s.l. Unlike other species, the amplitude of the nitrate concentration variation was very high (from 0.1 to  $14.8 \mu\text{g m}^{-3}$ ) between 1.1 and 2.5 km a.s.l. from 13:30 to 13:55 UTC (Fig. 9d). It can also be observed that the nitrate concentrations decreased quickly to  $0.1 \mu\text{g m}^{-3}$  at 0.5 km a.s.l. from 13:58 to 14:01 UTC. As reported by Crume rolle et al. (2013), peaks in nitrate may originate from natural (marine aerosol) or anthropogenic sources (industry exhaust). We note that Meso-NH reproduced the evolution and the magnitude of the concentration recorded onboard the ATR-42 over the Netherlands fairly correctly.

The observed mass concentration at Cabauw is compared to the simulated ones in Fig. 10. The evolution of the mass concentration recorded by the AMS (type: c-TOF) during the period from 25–30 May at Cabauw is marked by a signif-

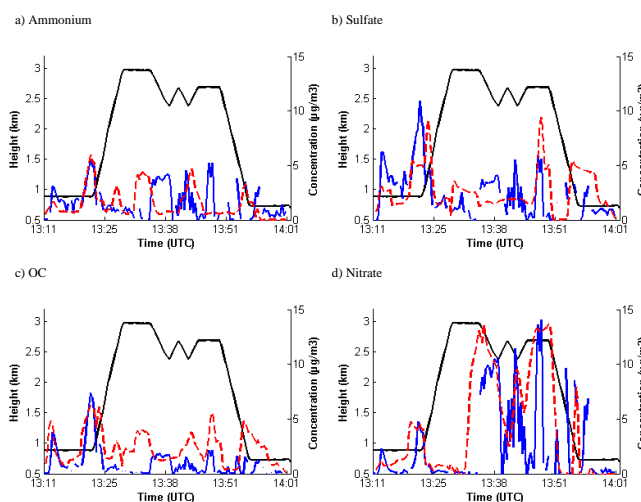


**Figure 9.** Evolution of (a) ammonium, (b) sulfate, (c) OC and (d) nitrate mass concentration ( $\mu\text{g m}^{-3}$ ) obtained from AMS measurements (blue solid line) and simulated (red dashed line) over the Netherlands between ( $52.57^\circ \text{ N}$ ,  $6.34^\circ \text{ E}$ ) and ( $51.88^\circ \text{ N}$ ,  $4.99^\circ \text{ E}$ ) on 30 May 2008. The black line indicates the height of the aircraft.

icant increase in the concentration on 30 May for the four species. We note that the evolution of the three inorganic salts (ammonium, sulfate, and nitrate) is fairly similar. First, the concentration of the inorganic salts increased from 25 to 27 May. Then it decreased on 28 May, before finally increasing rapidly again from 29 to 30 May (Fig. 10). The observed ammonium mass concentrations ranged from 0.5 to  $6 \mu\text{g m}^{-3}$  with the maximum appearing on 30 May (Fig. 10a). It can be also observed that the mass concentration of sulfate was less than that of the other species, with a maximum value of  $4.8 \mu\text{g m}^{-3}$ , also observed on 30 May (Fig. 10b). The evolution of the nitrate mass concentration was characterized by its wide range, extending from 0.1 to  $17 \mu\text{g m}^{-3}$ , observed on 28 and 30 May respectively (Fig. 10c). The evolution of the OC was characterized by a weak variability of the concentration compared to the inorganic salts. The OC mass concentration was confined between 1.6 and  $5 \mu\text{g m}^{-3}$ , except on 30 May where the concentration rose sharply to  $7.8 \mu\text{g m}^{-3}$  (Fig. 10d). It is also worth noting that Meso-NH reproduced the evolution of the concentrations acceptably well for the different chemical species measured by the AMS at Cabauw. Given that the AMS measurements are limited to refractive aerosol with diameter lower than 500 nm, we took from Meso-NH only the particles with diameter lower than 500 nm in order to compare them to the AMS measurements.

Both the observations and the simulation show that the air mass over the Netherlands on 30 May included a mixture of dust with the anthropogenic aerosol. The fraction of these different species considered as internally mixed was analyzed from the Meso-NH simulation. The results reveal that, near the surface at Cabauw and at altitude (between 1 and 3 km a.s.l.) around this site, the composition of the mixture

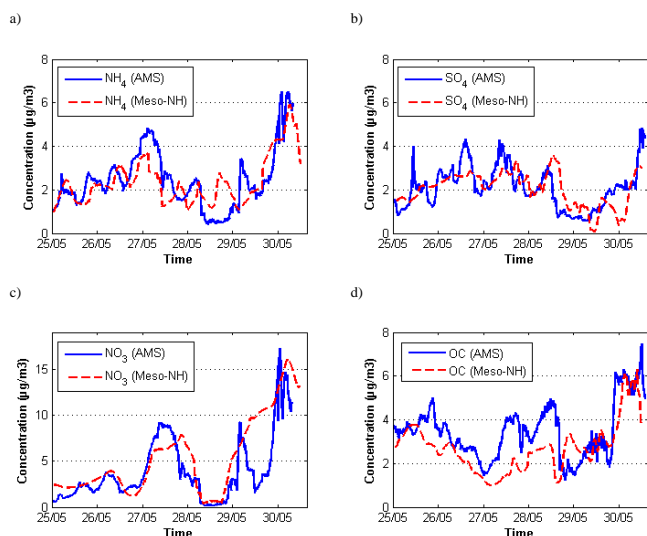


**Figure 10.** Evolution of (a) ammonium, (b) sulfate, (c) nitrate and (d) OC mass concentration ( $\mu\text{g m}^{-3}$ ) obtained from AMS measurements (blue solid line) and simulated (red dashed line) over Cabauw between 25 and 30 May 2008.

was fairly similar. More than 50 % of the mixture was made up of dust. The organic component represented an average of 15 % of the total mass, with the main contribution attributed to SOA ( $\sim 10$  % of the total mass). Despite of the mixing of the dust plume with BC and OC over Italy (Sect. 3.3), the contributions of BC and OC represented only 3.5 and 5 % on average respectively. The fraction of the inorganic salts was higher than the organic component, with 24.5 % on average. As expected on the basis of AMS observations, the fraction of nitrate obtained from Meso-NH simulation was more significant than that of the other inorganic salts, with values around 13.5 %. The fraction of sulphate and ammonium mixed with dust particles was estimated on average to 6 and 5 % respectively. Hence the major components were dust, followed by SOA and nitrate. Note that the simulated SOA concentrations were not compared to observations because of a lack of SOA observations over the Netherlands. Nonetheless, the chemical composition of the aerosol obtained as internally mixed was found to be consistent with previous studies of atmospheric processing of mineral dust particles in urban areas (Almeida et al., 2014; Reddington et al., 2013; Kumar et al., 2011; Stone et al., 2011; Putaud et al., 2004). The ability of these aged Saharan dust particles to act as CCN will be described in detail in Sect. 4.2.

#### 4.2 Hygroscopic properties of the dust plume

The chemical and physical processes and coating of inorganic salts (mainly sulfate and nitrate) change not only the mixing state and optical properties but also the hygroscopic properties of the aerosol (Leng et al., 2013; Rose et al., 2011; Wang et al., 2010; Jimenez et al., 2009; Reid et al., 1998).

Gibson et al. (2007) have shown that the CCN activity of insoluble mineral dust components is enhanced dramatically when they are internally mixed with a small amount of an aqueous salt. Thus, the heterogeneous reactions with reactive gases, including nitric, hydrochloric and sulfuric acids, can convert insoluble mineral dust into slightly soluble compounds or compounds that are sufficiently soluble to play an important role in hygroscopic growth and cloud droplet activation (Ram et al., 2014; Sullivan et al., 2009). The dust hygroscopicity is controlled by its chemical mixing state, which is determined by its mineralogy and the chemical reaction pathways it experiences during transport (Sullivan et al., 2009). According to these previous studies we can assume that the atmospheric processing of this Saharan dust has likely led to an evolution of its hygroscopicity.

The concentration of CCN in a given population of aerosol is a crucial parameter for understanding the ability of a particle to act as a nucleating agent. This ability depends on its size as well as the coating of hygroscopic species (Ram et al., 2014; Gunthe et al., 2011; Dusek et al., 2010; Sullivan et al., 2009). The CCN activity was effectively predicted using Köhler theory (Köhler, 1936) based on physico-chemical properties of the solute, such as its mass, molecular weight, density, size and activity coefficient. The CCN activity was calculated at the same supersaturation level that was chosen for making the measurements with the CCNC. The calculation was made by taking the simulated mass and number concentration of the different chemical species and their molecular weight into account, in addition to the simulated aerosol size. The evolution of the measured and simulated number concentration of CCN at 0.2 % supersaturation ( $\text{CCN}_{0.2}$ ) during the flight of the ATR-42 on 30 May from 13:11 to 14:01 UTC is shown in Fig. 11a. The simulated  $\text{CCN}_{0.2}$  concentration plotted in Fig. 11a was estimated from the aerosol accumulation and fine modes. The observed  $\text{CCN}_{0.2}$  concentration was relatively constant at around 80 particles  $\text{cm}^{-3}$  at 0.8 km a.s.l. from 13:11 to 13:25 UTC, and increased quickly thereafter to 700 particles  $\text{cm}^{-3}$  between 1 and 3 km a.s.l. Then, the observed concentration varied from 80 to 650 particles  $\text{cm}^{-3}$  between 2.8 and 3 km a.s.l., before reaching its maximum value (900 particles  $\text{cm}^{-3}$ ) at 2 km a.s.l. from 13:50 to 13:55 UTC (Fig. 11a). It can thus be observed that, on average, the lowest  $\text{CCN}_{0.2}$  concentration was mainly located near the surface. The comparisons between the CCN calculated and CCN observed following the altitude range (Fig. 12) reveal that the model is doing a good job over the boundary layer (1–2.4 and 2.5–3 km) with a correlation coefficient greater than 0.8. However, in the boundary layer where the concentrations are more sensitive to steep gradient of the surface emission, the CCN concentration is weakly reproduced by Meso-NH (coefficient correlation around to 0.4). In order to improve the results in the surface, the simulation should be run with better horizontal resolution (around 1 km) in agreement to the heterogeneities of the sources. Unfortunately, we haven't got a trustworthy



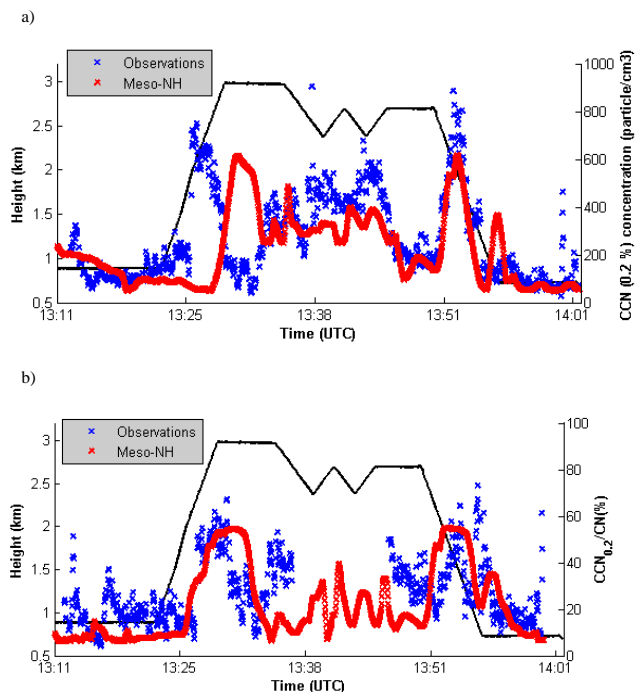


**Figure 11.** Evolution of (a) the CCN concentration and (b) the  $N_{CCN} / N_{CN}$  ratio at 0.2 % supersaturation obtained from CCNC and CN concentration (blue line) and calculated from the simulation (red line) over the Netherlands between (52.57° N, 6.34° E) and (51.88° N, 4.99° E) on 30 May 2008. The black line indicates the height of the aircraft.

emission inventory at these high resolutions. It is noteworthy that the evolution of the  $CCN_{0.2}$  concentration is predicted fairly well by taking the aged Saharan dust particles into account.

To characterize the relationship between  $CCN_{0.2}$  and total aerosol population in the atmospheric column, the  $CCN_{0.2} / CN$  ratio was calculated as a measure of hygroscopicity of the aerosol population (Fig. 11b). When its ratio is 0 %, no activation of aerosol can occur to form cloud droplets whereas, when its ratio reaches 100 %, all aerosol particles can be activated to become droplets. The measurements of the CPC 3010 were used to provide the CN concentration required to calculate the  $CCN_{0.2} / CN$  ratio. Unfortunately, CN concentrations were not recorded for the total length of the flight due to the presence of clouds. Most of the aerosol particles are found in a dominating and extremely broad accumulation mode. In general most of the particles (70–90 %) have sizes beyond 50 nm (not shown). Only for two smaller periods, one shortly after 13:15 UTC and the other around 13:55 UTC, smallest aerosol sizes in high number concentration (may stem from nucleation event) are observed.

The value of the  $CCN_{0.2} / CN$  ratio obtained from observations ranged between 10 and 70 %. The low values (less than 20 %) were mainly observed near the surface (0.7–1.5 km a.s.l.) whereas the maximum values of the ratio were

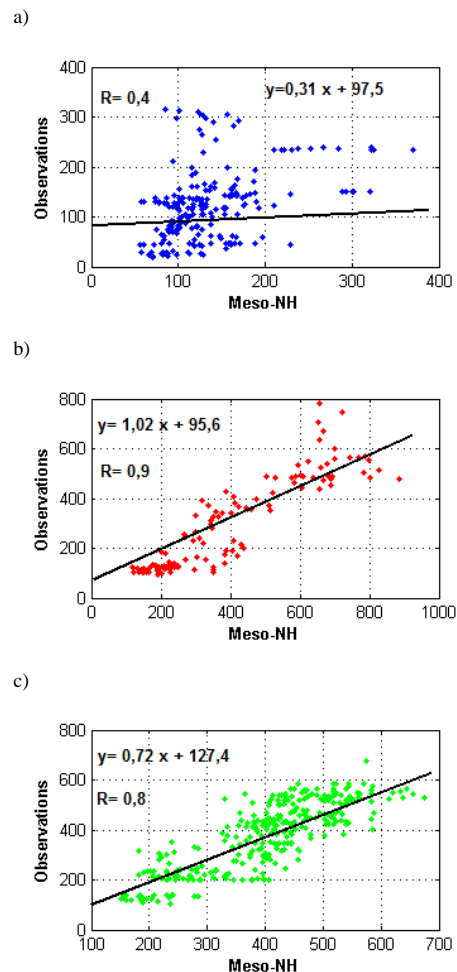


**Figure 12.** Scatterplot of the CCN evolution during the flight of the ATR-42 at (a) 0.5–0.9 km, (b) 1–2.4 km and (c) 2.5–3 km on 30 May 2008 over the Netherlands between 52.57° N, 6.34° E and 51.88° N, 4.99° E.

correlated with the maximum values of the  $CCN_{0.2}$  concentration. This is in agreement with the simulation results. In particular, it should be noted that the  $CCN_{0.2}$  concentration peak from 13:50 to 13:55 UTC was associated with the maximum value of the  $CCN_{0.2} / CN$  ratio (70 %). This was further corroborated by an enhancement in nitrate mass concentration (Fig. 9). The value of the  $CCN_{0.2} / CN$  ratio obtained was much greater than those observed over the Saharan region. During the AMMA campaign, the  $CCN/CN$  ratio obtained was less than 15 % in the Saharan Air Layer (Crumeirole et al., 2008). This reinforces our conclusion that heterogeneous reactions with inorganic salts converted this insoluble Saharan mineral dust into compounds that were sufficiently soluble to impact hygroscopic growth and cloud droplet activation over the Netherlands.

Figure 13 depicts the evolution of the measured and simulated number concentration of CCN at 0.16, 0.30, 0.45 and 0.63 % at Cabauw. A large, rapid increase in the number con-

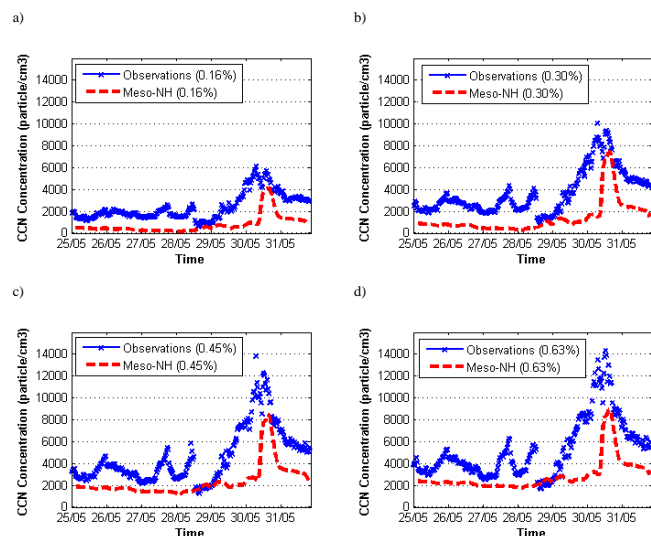


**Figure 13.** Evolution of the CCN concentration at water vapor supersaturation of (a) 0.16 %, (b) 0.30 %, (c) 0.45 % and (d) 0.63 % measured (blue line) and calculated from the simulation (red line) at Cabauw between 25 and 30 May 2008.

centration of the CCN can be observed for the four supersaturation levels between 29 and 31 May, with a maximum value of  $14\,000\text{ particles cm}^{-3}$  at 0.63 % supersaturation. The observed number concentration of CCN on 30 May was double the mean value observed during the EUCAARI-IMPACT campaign. Before 29 May, the CCN concentration at the four supersaturation levels was found to be fairly constant, except for the two weak peaks of CCN concentration observed on 27 and 28 May coinciding with higher BC mass concentration (Fig. 6). The simulated CCN concentration at Cabauw compared fairly well with the observations, and especially the high peak of CCN concentration, which was acceptably reproduced at the four supersaturation levels (Fig. 13). Indeed, on average more than 70 % of the CCN concentration observed on 30 May was found by Meso-NH. Nevertheless, we note the two weak peaks observed on 27 and 28 May are not found in the simulation. A possible source of this discrepancy could be an underestimation of BC mass concentration by Meso-NH on 27 and 28 May (Fig. 6). Using the chemical transport model GEOS-CHEM, Riipinen et al. (2011) have shown that organic components have a significant influence on the growth of ultrafine particles and in CCN production.

The high peak of CCN concentration observed on 30 May coincided with a significant increase in the mass concentration of inorganic salts (Fig. 10), in particular for nitrate. The simulation results reveal that more than 70 % of the CCN concentration observed on 30 May can be explained by the presence of the aged Saharan dust (Fig. 12). According to our simulation results mentioned above, we can conclude that the peak of CCN concentration observed on 30 May was mainly

due to the atmospheric processing of Saharan mineral dust particles.

The remaining 30 % could be attributed to other processes that can enhance the dust hygroscopicity, such as cloud processing, which is not taken into account in the simulations. Gibson et al. (2007) revealed that interaction between raindrops and the dust particles, both in and around clouds, may lead to the formation of new particles that are sufficiently hygroscopic to impact cloud droplet activation. Crumeyrolle et al. (2008) showed an increase in dust hygroscopicity over Niger by cloud processing in a mesoscale convective system. The composition of dust particles can also be significantly altered depending on the presence of cloud along their long-range transport (Matsuki et al., 2010). Thus, given the meteorological situation, we cannot ignore a possible influence of cloud processing on the hygroscopic properties of Saharan dust.

## 5 Summary and conclusion

The atmospheric processing of Saharan mineral dust particles during the EUCAARI intensive observational period has been presented in this study. An intense Saharan dust plume was transported toward northwestern Europe in a meteorological situation disturbed by strong convective activity over central Europe between 25 and 31 May 2008. The analysis focuses on the site of Cabauw, which was selected to quantify the regional aerosol properties, formation, transformation, transport and deposition during the EUCAARI 2008 campaign. The transport of dust to northwestern Europe was investigated by combining satellite, airborne and ground-based observations, and the non-hydrostatic mesoscale model Meso-NH. Through the use of this numerical model, it was well-identified that the dust coming from the western and central Sahara reached northern Europe. Moreover, the shape and temporal distribution of the dust plume simulated by Meso-NH was consistent with other simulations using different models (Bangert et al., 2012; Pappalardo et al., 2010). The altitude of the dust plume during its transport to northwestern Europe was assessed by using the CALIPSO observations. The depolarization ratio in the plume confirmed that the major dust plume was transported over Europe between 2 and 5 km a.s.l. Due to transport, the plume split into two layers over northern Europe. The simulation results have shown the mixing of the European pollution aerosol with dust particles in the lower layer. In agreement with Hamburger et al. (2011), it was shown that the most intense anthropogenic aerosol concentration was mainly located over northern Europe. The simulations revealed that the dust particles were mainly mixed with inorganic salts over Belgium and the Netherlands. In contrast, it was well identified from the simulation that the plume was mainly mixed with carbonaceous matter over Italy, likely leading to the adsorption of organic gases onto dust particles.

From the LNG observations onboard the ATR-42, the vertical structure of the aerosol layer over the Netherlands was assessed. The main aerosol layer was located between 1.8 and 2.5 km a.s.l., and the presence of aerosol was probed between 0.6 and 0.7 km a.s.l. in spite of the presence of clouds. The Meso-NH simulations were in fairly good agreement with the LNG and AMS observations. Small depolarization and color ratios derived from LNG measurements shows that the extinction coefficient was mainly due to the Saharan dust. The presence of the dust plume over the Netherlands led to an enhancement of the accumulation mode particle number concentration in both BL and LFT, which was found to be in agreement with Crumeyrolle et al. (2013). The analyses of the simulation have shown that mineral dust particles accumulated soluble material through internal mixing over the Netherlands. It results that the major components of the mixture were dust, followed by SOA and nitrate. The value of the  $\text{CCN}_{0.2} / \text{CN}$  ratio obtained over the Netherlands ( $\sim 70\%$ ) was much greater than those reported in the literature over the Saharan region (Matsuki et al., 2010; Crumeyrolle et al., 2008). In addition, the maximum of the  $\text{CCN}_{0.2} / \text{CN}$  ratio was correlated with the maximum values of the  $\text{CCN}_{0.2}$  concentration. This demonstrates that heterogeneous reactions with inorganic salts converted this Saharan mineral dust into compounds sufficiently soluble to impact the hygroscopic growth and cloud droplet activation over this region. The CCN measurement at Cabauw revealed a peak of the number concentration of CCN on 30 May, with a maximum of 14 000 particles  $\text{cm}^{-3}$  at 0.63 % supersaturation. As a result of the simulated CCN concentration, on average, more than 70 % of the CCN concentration observed on 30 May can be explained by the presence of the Saharan aged dust. Thus, the atmospheric processing of Saharan dust is shown to be the main process by which this peak of CCN was produced. It is also known that, during the cloud processing, the mineral dust can enhance its hygroscopic properties through a series of additional processes including chemical reaction in the aqueous phase (Smoydzin et al., 2012; Sullivan et al., 2007; Matsuki et al., 2010). Further analysis of the dust microphysical properties, including chemical reaction in the aqueous phase, will be examined in a forthcoming study. In conclusion, our results confirm that changes in dust chemical composition due to atmospheric aging can play a significant role in determining the CCN activity.

**Acknowledgements.** This work was partially funded by the European Commission 6th Framework program project EUCAARI and by the French National Research Agency (ANR) under the AEROCLOUD program. The authors also thank the TNO for providing the high resolution emission inventory used for this study. The authors would especially like to thank the staff of the team working on the airborne measurements aboard the ATR-42 during the EUCAARI campaign. In particular, Alfons Schwarzenboeck from LAMP (a.schwarzenboeck@opgc.univ-bpclermont.fr) is acknowledged for providing AMS, CPC and CCNC mea-

surements performed aboard the ATR-42. Jacques Pelon from LATMOS (jacques.pelon@latmos.ipsl.fr) is also acknowledged for LNG data. The MAAP data over the EUSAAR sites (Mont Cimone, Puy-de-Dôme and Hohenpeißenberg) were provided by EBAS database center (<http://ebas.nilu.no>). The MAAP data over Cabauw were provided by the EUCAARI IOP center (<http://www.knmi.nl/eucaari>). The authors would like to acknowledge CESAR database center (<http://www.cesar-database.nl>), Boers Reinout and Greg Roberts for the CCN concentration data over Cabauw. The CALIPSO products were provided by the ICARE center (<http://www.icare.univ-lille1.fr>). Simulations were performed on the CINES supercomputer. We thank the Meso-NH assistance team for their help and availability. We are also grateful to the CCUR team for the use of the TITAN supercomputer. The authors thank the editor Yinon Rudich and anonymous reviewers for very helpful reviews and relevant suggestions.

Edited by: Y. Rudich

## References

- Abdul-Razzak, H. and Ghan, S.: A parameterization of aerosol activation 2. Multiple aerosol types, *J. Geophys. Res.*, 105, 6837–6844, 2000.
- Abdul-Razzak, H. and Ghan, S.: Parameterization of the influence of organic surfactants on aerosol activation, *J. Geophys. Res.*, 109, D03205, doi:10.1029/2003JD004043, 2004.
- Almeida, G. P., Brito, J., Morales, C. A., Andrade, M. F., and Artaxo, P.: Measured and modelled cloud condensation nuclei (CCN) concentration in São Paulo, Brazil: the importance of aerosol size-resolved chemical composition on CCN concentration prediction, *Atmos. Chem. Phys.*, 14, 7559–7572, doi:10.5194/acp-14-7559-2014, 2014.
- Ansmann, A., Bosenberg, J., Chaikovskiy, A., Comeron, A., Eckhardt, S., Eixmann, R., Freudenthaler, V., Ginoux, P., Komguem, L., Linne, H., Marquez, M., Matthias, V., Mattis, I., Mittev, V., Müller, D., Music, S., Nickovic, S., Pelon, J., Sauvage, L., Sobolewsky, P., Srivastava, M., Sthol, A., Toress, O., Vaughan, G., Wandinger, U., and Wiegner, M.: Long-range transport to saharan dust to northern europe: The 11–16 october 2001 outbreak observed with earlinet, *J. Geophys. Res.*, 108, D124345, doi:10.1029/2003JD003757, 2003.
- Ansmann, A., Petzold, A., Kandler, K., Tegen, I., Wendisch, M., Müller, D., Weinzierl, B., Müller, T., and Heintzenberg, J.: Saharan mineral dust experiments samum-1 and samum-2: what have we learned?, *Tellus*, 63B, 403–429, 2011.
- Aouizerats, B., Thouaron, O., Tulet, P., Mallet, M., Gomes, L., and Henzing, J. S.: Development of an online radiative module for the computation of aerosol optical properties in 3-D atmospheric models: validation during the EUCAARI campaign, *Geosci. Model Dev.*, 3, 553–564, doi:10.5194/gmd-3-553-2010, 2010.
- Aouizerats, B., Tulet, P., Pigeon, G., Masson, V., and Gomes, L.: High resolution modelling of aerosol dispersion regimes during the CAPITOUL field experiment: from regional to local scale interactions, *Atmos. Chem. Phys.*, 11, 7547–7560, doi:10.5194/acp-11-7547-2011, 2011.

- Aouizerats, B., Tulet, P., and Gomes, L.: 3-D direct impacts of urban aerosols on dynamics during the capitoul field experiment, *Geophys. Res. Lett.*, 39, L23807, doi:10.1029/2012GL053781, 2012.
- Archer, D. and Johnson, K.: A model of the iron cycle in the ocean, *Global Biogeochem. Cy.*, 14, 269–279, doi:10.1029/1999GB900053, 2000.
- Baklanov, A., Laurence, M., and Pandis, S.: MEGAPOLI Description of Work (2008–2011), Copenhagen, ISBN978-87-992924-0-0, 2008.
- Bangert, M., Kottmeier, C., Vogel, B., and Vogel, H.: Regional scale effects of the aerosol cloud interaction simulated with an online coupled comprehensive chemistry model, *Atmos. Chem. Phys.*, 11, 4411–4423, doi:10.5194/acp-11-4411-2011, 2011.
- Bangert, M., Nenes, A., Vogel, B., Vogel, H., Barahona, D., Karydis, V. A., Kumar, P., Kottmeier, C., and Blahak, U.: Saharan dust event impacts on cloud formation and radiation over Western Europe, *Atmos. Chem. Phys.*, 12, 4045–4063, doi:10.5194/acp-12-4045-2012, 2012.
- Baray, J.-L., DufLOT, V., Posny, F., Cammas, J.-P., Thompson, A., Gabarrot, F., Bonne, J.-L., and Zeng, G.: One year ozonesonde measurements at kerguelen island (49.2° S, 70.1° E): Influence of stratosphere-to-troposphere exchange and long-range transport of biomass burning plumes, *J. Geophys. Res.*, 117, D06305, doi:10.1029/2011JD016717, 2012.
- Barthe, C., Molinié, G., and Pinty, J.: Description and first results of an explicit electrical scheme in a 3d cloud resolving model, *Atmos. Res.*, 76, 95–113, 2005.
- Bauer, S., Balkanski, Y., Schulz, M., Hauglustaine, D., and Dentener, F.: Global modeling of heterogeneous chemistry on mineral aerosol surface: 1. the influence on tropospheric ozone chemistry and comparison to observations, *J. Geophys. Res.*, 109, D02304, doi:10.1029/2003JD003868, 2004.
- Bauer, S. E., Menon, S., Koch, D., Bond, T. C., and Tsigaridis, K.: A global modeling study on carbonaceous aerosol microphysical characteristics and radiative effects, *Atmos. Chem. Phys.*, 10, 7439–7456, doi:10.5194/acp-10-7439-2010, 2010.
- Bechtold, P., Redelsperger, J.-L., Guichard, F., Hoff, C., Beau, I., Blackbrun, M., Brinkop, S., Grandpeix, J.-Y., Grant, A., Gregory, D., and Ioannidou, E.: A GCSO intercomparison for a tropical squall line observed during TOGA-COARE. II: Intercomparison of single-column models and a cloud-resolving model, *Q. J. Roy. Meteor. Soc.*, 126, 865–888, 2000.
- Bechtold, P., Bazile, E., Guichard, F., Mascart, P., and Richard, E.: A mass-flux convection scheme for regional and global models, *Q. J. Roy. Meteor. Soc.*, 127, 869–886, 2001.
- Bègue, N., Tulet, P., Chaboureaud, J.-P., Roberts, G., Gomes, L., and Mallet, M.: Long-range transport of saharan dust over northwestern europe during eucaari 2008 campaign: Evolution of dust optical properties by scavenging, *J. Geophys. Res.*, 117, D17201, doi:10.1029/2012JD017611, 2012.
- Bougeault, P. and Lacarrere, P.: Parameterization of orography-induced turbulence in a meso-beta model, *Mon. Weather Rev.*, 117, 1872–1890, 1989.
- Bou Karam, D., Flamant, C., Tulet, P., Todd, M., Pelon, P., and Williams, E.: Dry cyclogenesis and dust mobilization in the intertropical discontinuity of the west Africa monsoon: A case study, *J. Geophys. Res.*, 114, D05115, doi:10.1029/2008JD010952, 2009.
- Canagaratna, M., Jayne, J., Jimenez, J., Allan, J., Alfarra, M., Zhang, Q., Onasch, T., Drewnick, F., Coe, H., Middelbrook, A., Delia, A., Williams, L., Trinborn, A., Northway, M., DeCarlo, P., Kolb, C., Davidovits, P., and Worsnop, D.: Chemical and microphysical characterization of ambient aerosols with the aerodyne aerosol mass spectrometer, *Mass Spectrom. Rev.*, 26, 185–222, 2007.
- Caqueneau, S., Gaudichet, A., Gomes, L., and Legrand, M.: Mineralogy of Saharan dust transported over northwestern tropical atlantic ocean in relation to source, *J. Geophys. Res.*, 107, AAC4-1–AAC4-12 doi:10.1029/2000JD000247, 2002.
- Catrrall, C., Reagan, J., Thome, K., and Dubovik, O.: Variability of aerosol and spectral lidar and backscatter and extinction ratios of key aerosol types derived from selected Aerosol Robotic Network locations, *J. Geophys. Res.*, 110, D10S11 doi:10.1029/2004JD005124, 2005.
- Chaboureaud, J., Richard, E., Pinty, J., Flamant, C., Girolamo, P. D., Kiemle, C., Behrendt, A., Chepfer, H., Chiriaco, M., and Wulfmeyer, V.: Long-range transport of Saharan dust and its radiative impact on precipitation forecast over western Europe: a case study during the Convective and Orographically induced Precipitation Study (COPS), *Q. J. Roy. Meteor. Soc.*, 137, 236–251, 2011.
- Chen, L.-L., Carmichael, G., Hong, M., Ueda, H., Shim, S., Song, C., Kim, Y., Arimoto, R., Prospero, J., Savoie, D., Murano, K., Park, J., Lee, H., and Kang, C.: Influence of continental outflow events on the aerosol composition at Cheju Island, South Korea, *J. Geophys. Res.*, 102, doi:10.1029/97JD01431, 1997.
- Chou, C., Stetzer, O., Weingartner, E., Jurányi, Z., Kanji, Z. A., and Lohmann, U.: Ice nuclei properties within a Saharan dust event at the Jungfraujoch in the Swiss Alps, *Atmos. Chem. Phys.*, 11, 4725–4738, doi:10.5194/acp-11-4725-2011, 2011.
- Clain, G., Baray, J.-L., Delmas, R., Keckhut, P., and Cammas, J.-P.: A lagrangian approach to analyse the tropospheric ozone climatology in the tropics: Climatology of stratosphere-troposphere exchange at reunion island, *Atmos. Environ.*, 44, 968–975, 2010.
- Cohard, J. and Pinty, J.: A comprehensive two-moment warm microphysical bulk scheme, II: 2-D experiments with a non hydrostatic model, *Q. J. Roy. Meteor. Soc.*, 126, 1843–1859, 2000.
- Cohard, J., Pinty, J., and Suhre, K.: On the parameterization of activation spectra from cloud condensation nuclei microphysical properties, *J. Geophys. Res.*, 105, 11753–11766, 2000.
- Collaud Coen, M., Weingartner, E., Schaub, D., Hueglin, C., Corrigan, C., Henning, S., Schwikowski, M., and Baltensperger, U.: Saharan dust events at the Jungfraujoch: detection by wavelength dependence of the single scattering albedo and first climatology analysis, *Atmos. Chem. Phys.*, 4, 2465–2480, doi:10.5194/acp-4-2465-2004, 2004.
- CrumeYrolle, S., Gomes, L., Tulet, P., Matsuki, A., Schwarzenboeck, A., and Crahan, K.: Increase of the aerosol hygroscopicity by cloud processing in a mesoscale convective system: a case study from the AMMA campaign, *Atmos. Chem. Phys.*, 8, 6907–6924, doi:10.5194/acp-8-6907-2008, 2008.
- CrumeYrolle, S., Manninen, H. E., Sellegri, K., Roberts, G., Gomes, L., Kulmala, M., Weigel, R., Laj, P., and Schwarzenboeck, A.: New particle formation events measured on board the ATR-42 aircraft during the EUCAARI campaign, *Atmos. Chem. Phys.*, 10, 6721–6735, doi:10.5194/acp-10-6721-2010, 2010.

- Crumeyrolle, S., Schwarzenboeck, A., Roger, J. C., Sellegri, K., Burkhart, J. F., Stohl, A., Gomes, L., Quennehen, B., Roberts, G., Weigel, R., Villani, P., Pichon, J. M., Bourrianne, T., and Laj, P.: Overview of aerosol properties associated with air masses sampled by the ATR-42 during the EUCAARI campaign (2008), *Atmos. Chem. Phys.*, 13, 4877–4893, doi:10.5194/acp-13-4877-2013, 2013.
- Cuesta, J., Edouard, D., Mimouni, M., Flamant, P., Loth, C., Gibert, F., Marnas, F., Bouklila, A., Kharef, M., Ouchène, B., Kadi, M., and Flamant, C.: Multiplatform observations of the seasonal evolution of the saharan atmospheric boundary layer in Tamanrasset, Algeria, in the framework of the African monsoon multidisciplinary analysis field campaign conducted in 2006, *J. Geophys. Res.*, 113, D00C07 doi:10.1029/2007JD009417, 2008.
- DeMott, P., Sassen, K., Poellot, M., Baumgardner, D., Rogers, D., Brooks, S., Prenni, A., and Kreidenweis, S.: African dust aerosols as atmospheric ice nuclei, *Geophys. Res. Lett.*, 30, 1732, doi:10.1029/2003GL017410, 2003.
- de Villiers, R. A., Ancellet, G., Pelon, J., Quennehen, B., Schwarzenboeck, A., Gayet, J. F., and Law, K. S.: Airborne measurements of aerosol optical properties related to early spring transport of mid-latitude sources into the Arctic, *Atmos. Chem. Phys.*, 10, 5011–5030, doi:10.5194/acp-10-5011-2010, 2010.
- Duflot, V., Dils, B., Baray, J.-L., Mazire, M. D., Attié, J.-L., Vanhaelewyn, G., Senten, C., Vigouroux, C., Clain, G., and Delmas, R.: Analysis of the origin of the distribution of co in the subtropical southern indian ocean in 2007, *J. Geophys. Res.*, 115, D22106, doi:10.1029/2010JD013994, 2010.
- Dufour, A., Amodei, M., Ancellet, G., and Peuch, V. H.: Observed and modeled chemical weather during escompte, *Atmos. Res.*, 74, 161–189, 2004.
- Dusek, U., Frank, G., Hildebrandt, L., Curtius, J., Schneider, J., Walter, S., Chand, D., Drewnick, F., Jung, S., Borrmann, S., and Andreae, M.: Size matters more than chemistry for cloud-nucleating ability for aerosol particles, *Science*, 312, 1375–1378, 2006.
- Dusek, U., Frank, G., Curtius, J., Drewnick, F., Schneider, J., Kürten, A., Rose, D., Andreae, M., Borrmann, S., and Pöschl, U.: Enhanced organic mass fraction and decreased hygroscopicity of cloud condensation nuclei (CCN) during new particle formation events, *Geophys. Res. Lett.*, 37, L03804, doi:10.1029/2009GL040930, 2010.
- Engelstaedter, S. and Washington, R.: Atmospheric controls on the annual cycle of north african dust, *J. Geophys. Res.*, 112, D03103, doi:10.1029/2006JD007195, 2007.
- Engelstaedter, S., Tegen, I., and Washington, R.: North african dust emission and transport, *Earth Sci. Rev.*, 79, 73–100, 2006.
- Falkovich, A., Ganor, E., Levin, Z., Formenti, P., and Rudich, Y.: Chemical and mineralogical analysis of individual mineral dust particles, *J. Geophys. Res.*, 106, 18029–18036, doi:10.1029/2000JD900430, 2001.
- Fernald, F. G.: Analysis of atmospheric lidar observations – Some comments, *Appl. Opt.*, 23, 652–653, 1984.
- Forster, P.: Change in atmospheric constituents and in radiative forcing, in: *Climate Change 2007: The physical Science Basis, Contribution of Working Group I to the Fourth Assessment Report of the IPCC*, Cambridge University Press, 2007.
- Ghan, S., Abdul-Razzak, H., Nenes, A., Ming, Y., Liu, X., Ovchinnikov, M., Shipway, B., Meskhidze, N., Xu, J., and Shi, X.: Droplet nucleation: Physically-based parameterizations and comparative evaluation, *J. Adv. Model. Earth. Syst.*, 3, M10001, doi:10.1029/2011MS000074, 2011.
- Ghan, S., Smith, S., Wang, M., Zhang, K., Pringle, K., Carslaw, K., Pierce, J., Bauer, S., and Adams, P.: A simple model of global aerosol indirect effects, *J. Geophys. Res.*, 118, 6688–6707, doi:10.1002/jgrd.50567, 2013.
- Gibson, E., Gierlus, K., Hudson, P., and Grassian, V.: Generation of interbally mixed insoluble and soluble aerosol particles to investigate the impact of atmospheric aging and heterogeneous processing on the CCN activity of mineral dust aerosol, *Aerosol. Sci. Tech.*, 41, 914–924, doi:10.1080/02786820701557222, 2007.
- Ginoux, P., Prospero, J., Torres, O., and Chin, M.: Long-term simulation of global distribution with the gocart model: correlation with north atlantic oscillation, *Environ. Modell. Softw.*, 19, 113–128, 2004.
- Goudie, A.: Desert dust and human health disorders, *Env. Int.*, 63, 101–113, doi:10.1016/j.envint.2013.10.011, 2014.
- Goudie, A. and Middleton, N.: Saharan dust storms: nature and consequences, *Earth Sci. Rev.*, 56, 179–204, 2001.
- Griffin, R., Dabdub, D., and Seinfeld, J.: Secondary organic aerosol. 1. Atmospheric chemical mechanism for production of molecular constituents, *J. Geophys. Res.*, 107, 4332, doi:10.1029/2001JD000541, 2002.
- Griffin, R., Dabdub, D., and Seinfeld, J.: Development and initial evaluation of a dynamic species-resolved model for gas phase chemistry and size-resolved gas/particle partitioning associated with secondary organic aerosol formation, *J. Geophys. Res.*, 110, D05304, doi:10.1029/2004JD005219, 2005.
- Grini, A., Tulet, P., and Gomes, L.: Dusty weather forecast using the MesoNH atmospheric model, *J. Geophys. Res.*, 111, D19205, doi:10.1029/2005JD007007, 2006.
- Gunthe, S. S., Rose, D., Su, H., Garland, R. M., Achtert, P., Nowak, A., Wiedensohler, A., Kuwata, M., Takegawa, N., Kondo, Y., Hu, M., Shao, M., Zhu, T., Andreae, M. O., and Pöschl, U.: Cloud condensation nuclei (CCN) from fresh and aged air pollution in the megacity region of Beijing, *Atmos. Chem. Phys.*, 11, 11023–11039, doi:10.5194/acp-11-11023-2011, 2011.
- Hamburger, T., McMeeking, G., Minikin, A., Birmili, W., Dall'Osto, M., O'Dowd, C., Flentje, H., Henzing, B., Junninen, H., Kristensson, A., de Leeuw, G., Stohl, A., Burkhart, J. F., Coe, H., Krejci, R., and Petzold, A.: Overview of the synoptic and pollution situation over Europe during the EUCAARI-LONGREX field campaign, *Atmos. Chem. Phys.*, 11, 1065–1082, doi:10.5194/acp-11-1065-2011, 2011.
- Hatch, C., Gierlus, K., Schuttelefield, J., and Grassian, V.: Water adsorption and cloud condensation nuclei activity of calcite and calcite coated with model humic and fulvic acids, *Atmos. Environ.*, 42, 5672–5684, 2008.
- Haywood, J. and Boucher, O.: Estimates of the direct and indirect radiative forcing due to tropospheric aerosols: A review, *Rev. Geophys.*, 38, 513–543, 2000.
- Jickells, T.: Global iron connections: Between desert dust, ocean biogeochemistry and climate, *Science*, 308, 67–71, 2005.
- Jimenez, J., Canagaratna, M., Donahue, N. M., Prevot, A. S. H., Zhang, Q., Kroll, J. H., DeCarlo, P. F., Allan, J. D., Coe, H., Ng, N. L., Aiken, A. C., Docherty, K. S., Ulbrich, I. M., Grieshop, A. P., Robinson, A. L., Duplissy, J., Smith, J. D., Wilson, K. R., Lanz, V. A., Hueglin, C., Sun, Y. L., Tian, J., Laaksonen,



- A., Raatikainen, T., Rautiainen, J., Vaattovaara, P., Ehn, M., Kulmala, M., Tomlinson, J. M., Collins, D. R., Cubison, M. J., Dunlea, E. J., Huffman, J. A., Onasch, T. B., Alfarra, M. R., Williams, P. I., Bower, K., Kondo, Y., Schneider, J., Drewnick, F., Borrmann, S., Weimer, S., Demerjian, K., Salcedo, D., Cottrell, L., Griffin, R., Takami, A., Miyoshi, T., Hatakeyama, S., Shimono, A., Sun, J. Y., Zhang, Y. M., Dzepina, K., Kimmel J. R., Sueper, D., Jayne, J. T., Herndon, S. C., Trimborn, A. M., Williams, L. R., Wood, E. C., Middlebrook, A. M., Kolb, C. E., Baltensperger, U. and Worsnop, D. R.: Evolution of organic aerosols in the atmosphere, *Science*, 326, 1525–1529, 2009.
- Kain, J. and Fritsch, J.: Convective parameterization for mesoscale models: The kain-fitsch scheme, in: *The representation of cumulus convection in numerical models*, edited by: Emanuel, K. A. and Raymond, D. J., AMS, Monographs, 201 Charles Street, Providence, RI 02904-2294 USA, 46, 165–170, 1993.
- Kelly, T., Chuang, C., and Wexler, A.: Influence of dust composition on cloud droplet formation, *Atmos. Environ.*, 41, 2904–2916, 2007.
- Klein, H., Nickovic, S., Haunold, W., Bundke, U., Nillius, B., Ebert, M., Weinbruch, S., Schuetz, L., Levin, Z., Barrie, L. A., and Bingemer, H.: Saharan dust and ice nuclei over Central Europe, *Atmos. Chem. Phys.*, 10, 10211–10221, doi:10.5194/acp-10-10211-2010, 2010.
- Klett, J.: Lidar inversion with variable backscatter / extinction ratios, *Appl. Opt.*, 24, 1638–1643, 1985.
- Koehler, K., Kreidenweis, S. M., DeMott, P. J., Petter, M. D., Prenni, A. J., and Carrico, C. M.: Hygroscopicity and cloud droplet activation of mineral dust aerosol, *Geophys. Res. Lett.*, 36, L08805, doi:10.1029/2009GL037348, 2009.
- Koehler, K. A., Kreidenweis, S. M., DeMott, P. J., Petters, M. D., Prenni, A. J., and Möhler, O.: Laboratory investigations of the impact of mineral dust aerosol on cold cloud formation, *Atmos. Chem. Phys.*, 10, 11955–11968, doi:10.5194/acp-10-11955-2010, 2010.
- Köhler, H.: The nucleus in and the growth of hygroscopic droplets, *T. Faraday Soc.*, 32, 1152–1161, 1936.
- Kulmala, M., Asmi, A., Lappalainen, H. K., Carslaw, K. S., Pöschl, U., Baltensperger, U., Hov, Ø., Brenquier, J.-L., Pandis, S. N., Facchini, M. C., Hansson, H.-C., Wiedensohler, A., and O'Dowd, C. D.: Introduction: European Integrated Project on Aerosol Cloud Climate and Air Quality interactions (EUCAARI) – integrating aerosol research from nano to global scales, *Atmos. Chem. Phys.*, 9, 2825–2841, doi:10.5194/acp-9-2825-2009, 2009.
- Kumar, P., Sokolik, I. N., and Nenes, A.: Measurements of cloud condensation nuclei activity and droplet activation kinetics of fresh unprocessed regional dust samples and minerals, *Atmos. Chem. Phys.*, 11, 3527–3541, doi:10.5194/acp-11-3527-2011, 2011.
- Lafore, J. P., Stein, J., Asencio, N., Bougeault, P., Ducrocq, V., Duron, J., Fischer, C., Hérel, P., Mascart, P., Masson, V., Pinty, J. P., Redelsperger, J. L., Richard, E., and Vilà-Guerau de Arellano, J.: The Meso-NH Atmospheric Simulation System. Part I: adiabatic formulation and control simulations, *Ann. Geophys.*, 16, 90–109, doi:10.1007/s00585-997-0090-6, 1998.
- Laurent, B., Marticorena, B., Bergametti, G., Lon, J., and Mahowald, N.: Modeling mineral dust emissions from the saharan desert using new surface properties and soil database, *J. Geophys. Res.*, 113, D14218, doi:10.1029/2007JD009484, 2008.
- Leng, C., Cheng, T., Chen, J., Zhang, R., Tao, J., Huang, G., Zha, S., Zhang, M., Fang, W., Li, X., and Li, L.: Measurements of surface cloud condensation nuclei and aerosol activity in downtown shanghai, *Atmos. Environ.*, 69, 354–361, 2013.
- Levin, Z., Ganor, E., and Gladstein, V.: The effects of desert particles coated with sulfate on rain formation in the eastern mediterranean, *J. Appl. Meteorol.*, 35, 1511–1523, 1996.
- Levin, Z., Wurzler, S., Ganor, E., Ying, Y., and Teller, A.: On the modification of mineral dust particles based on their path of transport and the effect on mixed phase clouds and precipitation, *J. Aerosol Sci.*, 32, 1511–1523, 2001.
- Li, W. J. and Shao, L. Y.: Observation of nitrate coatings on atmospheric mineral dust particles, *Atmos. Chem. Phys.*, 9, 1863–1871, doi:10.5194/acp-9-1863-2009, 2009.
- Marticorena, B. and Bergametti, G.: Modelling of the atmospheric dust cycle: 1. design of a soil derived dust emission scheme, *J. Geophys. Res.*, 100, 16415–16429, 1995.
- Matsuki, A., Schwarzenboeck, A., Venzac, H., Laj, P., Crumeyrolle, S., and Gomes, L.: Cloud processing of mineral dust: direct comparison of cloud residual and clear sky particles during AMMA aircraft campaign in summer 2006, *Atmos. Chem. Phys.*, 10, 1057–1069, doi:10.5194/acp-10-1057-2010, 2010.
- McNaughton, C., Clarke, A., Howell, S., Pinkerton, M., Anderson, B., Thornhill, L., Hudgins, C., Winstead, E., Dibb, J., Scauer, E., and Maring, H.: Results from the inlet characterization experiment (dice): Airborne versus surface sampling of mineral dust and sea salt aerosols, *Aerosol. Sci. Tech.*, 41, 136–159, 2007.
- Mertes, S., Schroeder, F., and Wiedensohler, A.: The particle detection efficiency curve of the tsi3010 cpc as a function of temperature difference between saturator and condenser, *Aerosol. Sci. Tech.*, 23, 257–270, 1995.
- Metzger, S., Dentener, F., Pandis, S., and Lelieveld, J.: Gas/aerosol partitioning: 1. A computationally efficient model, *J. Geophys. Res.*, 107, ACH16-1–ACH16-24, doi:10.1029/2001JD001102, 2002.
- Middlebrook, A., Bahreini, R., Jimenez, J., and Canagarathna M.: Evaluation of composition-dependent collection efficiencies for the aerodyne aerosol mass spectrometer using field data, *Aerosol. Sci. Tech.*, 46, 258–271, 2012.
- Mohwald, N., Baker, A., Bergametti, G., Brooks, N., Duce, R., Jickells, T., Kubilay, N., Prospero, J., and Tegen, I.: Atmospheric global dust cycle and iron inputs to the ocean, *Global Biogeochem. Cy.*, 19, GB4025, doi:10.1029/2004GB002402, 2005.
- Mokhtari, M., Gomes, L., Tulet, P., and Rezoug, T.: Importance of the surface size distribution of erodible material: an improvement on the Dust Entrainment And Deposition (DEAD) Model, *Geosci. Model Dev.*, 5, 581–598, doi:10.5194/gmd-5-581-2012, 2012.
- Mona, L., Amodeo, A., Pandofi, M., and Pappalardo, G.: Saharan dust intrusion in the mediterranean area: Three years of raman lidar measurements, *J. Geophys. Res.*, 111, D16203, doi:10.1029/2005JD006569, 2006.
- Noihlan, J. and Mahfouf, J.: The ISBA land surface parametrization scheme, *Global Planet. Change*, 13, 145–159, 1996.
- Papayannis, A., Amiridis, V., Mona, L., Tsaknakis, G., Balis, D., Bosenberg, J., Chaikovski, A., Tomasi, F. D., Grigorov, I., Mattis, I., Mitev, V., Muller, D., Nickovic, S., Perez, C., Pietruczuk, A.,

- Pisani, G., Ravetta, F., Rizi, V., Sicard, M., Trickl, T., Weigner, M., Manouri, R. G., D'Amico, G., and Pappalardo, G.: Systematic lidar observations of saharan dust over europe in the frame of eralinet (2000–2002), *J. Geophys. Res.*, 113, D10204, doi:10.1029/2007JD009028, 2008.
- Pappalardo, G., Wandinger, U., Mona, L., Hiebsch, A., Mattis, I., Amodeo, A., Ansmann, A., Seifert, P., Linne, H., Apituley, A., Arboledas, L., Balis, D., Chaikovskiy, A., D'Amico, G., Tomasi, F. D., Freudenthaler, V., Giannakaki, E., Guinta, A., Grigorov, I., Iarlori, M., Madonna, M., Mamori, R., Nasti, L., Papayannis, A., Pietruczuk, A., Pujadas, M., Rizi, V., Rocadenbosch, F., Russo, F., Scnell, F., Spinelli, N., Wang, X., and Wieger, M.: Earlinet correlative measurements for calipso: First intercomparison results, *J. Geophys. Res.*, 115, D00H19, doi:10.1029/JD012147, 2010.
- Pelon, J., Flamant, C., Chazette, P., Lon, J.-F., Tanré, D., Sicard, M., and Satheesh, S.: Characterization of aerosol spatial distribution and optical properties over the indian ocean from airborne lidar and radiometry during indoex'99, *J. Geophys. Res.*, 107, 8029, doi:10.1029/2001JD000402, 2002.
- Penner, J., Andreae, M., Annegarn, H., Barrie, L., Feichter, J., Hegg, D., Jayaraman, A., Leaitch, R., Murphy, D., Nganga, J., and Pitari, G.: Aerosols, their direct and indirect effects, *Climate Change: The scientific basis*, 289–349, edited by: Houghton, J. T., Ding, Y., Griggs, D. J., Noguer, M., Van der Linden, P. J., Dai, X., Maskell, K., and Johnson, C. A., Cambridge University Press, UK, 2001.
- Perry, D., Cliff, S., and Jimenez-Cruz, P.: Evidence for hygroscopic dust particles 1 from the intercontinental transport and chemical transformation experiment, *J. Geophys. Res.*, 109, D23S28, doi:10.1029/2004JD004979, 2004.
- Petzold, A. and Schronlinner, M.: Multi-angle absorption photometry – a new method for the measurement of aerosol light absorption and atmospheric black carbon, *J. Atmos. Sci.*, 35, 421–441, 2004.
- Pinty, J. and Jabouille, P.: A mixed-phase cloud parameterization for use in mesoscale non hydrostatic model: simulations of a squall line and of orographic precipitations, *Conference of Cloud Physics*, Everett, WA, USA, 217–220, 1998.
- Prospero, J., Ginoux, P., Torres, O., Nicholson, S., and Gill, T.: Environmental characterization of global sources of atmospheric soil dust identified with the nimbus 7 total ozone mapping spectrometer (TOMS) absorbing aerosol product, *Rev. Geophys.*, 40, 1002, doi:10.1029/2000RG000095, 2002.
- Putaud, J., Raes, F., Dingenen, R. V., Brüggemann, E., Fachini, M., Decesari, S., Fuzzi, S., Gehrig, R., Hglin, C., Laj, P., Lorbeer, G., Maenhaut, W., Mihalopoulos, N., Müller, K., Querol, X., Rodriguez, S., Schneider, J., Spindler, G., tenBrink, H., Torseth, K., and Wiedensohler, A.: A european aerosol phenomenology- 2: chemical characteristics of particle matter at kerbside, urban rural and background sites in europe, *Atmos. Environ.*, 38, 2579–2595, 2004.
- Ram, K., Tripathi, S., Sarin, M., and Bhattu, D.: Primary and secondary aerosols from an urban site (kanpur) in the indo-gangetic plain: Impact on ccn, cn concentrations and optical properties, *Atmos. Environ.*, 89, 655–663, 2014.
- Reddington, C. L., McMeeking, G., Mann, G. W., Coe, H., Frontoso, M. G., Liu, D., Flynn, M., Spracklen, D. V., and Carslaw, K. S.: The mass and number size distributions of black carbon aerosol over Europe, *Atmos. Chem. Phys.*, 13, 4917–4939, doi:10.5194/acp-13-4917-2013, 2013.
- Reid, J., Hobbs, P., Ferek, R., Blake, D., Martins, J., and Liousse, C.: Physical, chemical and optical properties of regional hazes dominated by smoke in Brazil, *J. Geophys. Res.*, 103, 32059–32080, 1998.
- Riipinen, I., Pierce, J. R., Yli-Juuti, T., Nieminen, T., Häkkinen, S., Ehn, M., Junninen, H., Lehtipalo, K., Petäjä, T., Slowik, J., Chang, R., Shantz, N. C., Abbatt, J., Leaitch, W. R., Kerminen, V.-M., Worsnop, D. R., Pandis, S. N., Donahue, N. M., and Kulmala, M.: Organic condensation: a vital link connecting aerosol formation to cloud condensation nuclei (CCN) concentrations, *Atmos. Chem. Phys.*, 11, 3865–3878, doi:10.5194/acp-11-3865-2011, 2011.
- Roberts, G. and Nenes, A.: A continuous-flow streamwise thermal-gradient ccn chamber for atmospheric measurements, *Aerosol. Sci. Tech.*, 39, 206–221, 2005.
- Roberts, G., Artaxo, P., Zhu, J., Swietlicki, E., and Andreae, M.: Sensitivity of ccn spectra on chemical and physical properties of aerosol: A case study from the amazon basin, *J. Geophys. Res.*, 107, 8070, doi:10.1029/2001JD000583, 2002.
- Roberts, G., Mauger, G., Hadley, O., and Ramanathan, V.: North american and asian aerosols over the eastern pacific ocean and their role in regulating cloud condensation nuclei, *J. Geophys. Res.*, 111, D13205, doi:10.1029/2005JD006661, 2006.
- Rose, D., Gunthe, S. S., Su, H., Garland, R. M., Yang, H., Berghof, M., Cheng, Y. F., Wehner, B., Achtert, P., Nowak, A., Wiedensohler, A., Takegawa, N., Kondo, Y., Hu, M., Zhang, Y., Andreae, M. O., and Pöschl, U.: Cloud condensation nuclei in polluted air and biomass burning smoke near the mega-city Guangzhou, China – Part 2: Size-resolved aerosol chemical composition, diurnal cycles, and externally mixed weakly CCN-active soot particles, *Atmos. Chem. Phys.*, 11, 2817–2836, doi:10.5194/acp-11-2817-2011, 2011.
- Sarthou, G., Baker, A., Blain, S., Achterberg, E., Boye, M., Bowie, A., Croot, P., Laan, P., de Baar, H., Jickells, T., and Worsfold, P.: Atmospheric iron deposition and sea surface dissolved iron concentrations in the eastern atlantic ocean, *Deep-Sea Res. Pt. I*, 50, 1339–1352, 2003.
- Sassen, K., DeMott, P., Prospero, J., and Poellot, M.: Saharan dust storms and indirect aerosol effects on clouds: Crystal-face results, *Geophys. Res. Lett.*, 30, 1633, doi:10.1029/2003GL017371, 2003.
- Schepanski, K., Tegen, I., Laurent, B., Heinold, B., and Macke, A.: A new Saharan dust source activation frequently map derived from msg-severi ir-channels, *Geophys. Res. Lett.*, 34, L18803, doi:10.1029/2007GL030168, 2007.
- Schepanski, K., Flamant, C., Chaboureaud, J.-P., Kocha, C., Banks, J., Brindley, H., Lavaysse, C., Marnas, F., Pelon, J., and Tulet, P.: Characterization of dust emission from alluvial sources using aircraft observations and high-resolution modeling, *J. Geophys. Res.*, 118, 7237–7259, doi:10.1002/jgrd.50538, 2013.
- Shulman, M., Jacobson, M., Charlson, R., Synovec, R., and Young, T.: Dissolution behavior and surface tension effects of organic compounds in nucleating cloud droplets, *Geophys. Res. Lett.*, 23, 277–280, 1996.
- Slinn, W.: Atmospheric sciences and power production, precipitation Scavenging, US Department of Energy, Washington, D.C., 1979.

- Smoydzin, L., Teller, A., Tost, H., Fnaiss, M., and Lelieveld, J.: Impact of mineral dust on cloud formation in a Saharan outflow region, *Atmos. Chem. Phys.*, 12, 11383–11393, doi:10.5194/acp-12-11383-2012, 2012.
- Song, X. and Zhang, G.: Microphysics parameterization for convective clouds in a global climate model: Description and single-column model tests, *J. Geophys. Res.*, 116, D02201, doi:10.1029/2010JD014833, 2011.
- Stith, J., Ramanathan, V., Cooper, W., Roberts, G., DeMott, P., Carmichael, G., Hatch, C., Adhikary, B., Twohy, C., Rogers, D., Baumgardner, D., Prenni, A., Campos, T., Gao, R., Anderson, J., and Feng, Y.: An overview of aircraft observations from the pacific dust experiment campaign, *J. Geophys. Res.*, 114, D05207, doi:10.1029/2008JD010924, 2009.
- Stone, E., Soon-Chang, Y., and Schauer, J.: Chemical characterization of fine and coarse particles in Gosan, Korea during spring-time dust events, *Aerosol Air Qual. Res.*, 11, 31–43, 2011.
- Suhre, K., Mari, C., Bates, T., Johnson, J., Rosset, R., Wang, Q., Bandy, A., Blake, D., Businger, S., Eisels, F., Huebert, B., Kok, G., Mauldin, R. I., Prévôt, A., Schillawski, R., Tanner, D., and Thornton, D.: Physico-chemical modeling of the first aerosol characterization experiment (ACE 1) lagrangian b, 1, a moving column approach, *J. Geophys. Res.*, 103, 16433–16455, 1998.
- Sullivan, R. C., Guazzotti, S. A., Sodeman, D. A., and Prather, K. A.: Direct observations of the atmospheric processing of Asian mineral dust, *Atmos. Chem. Phys.*, 7, 1213–1236, doi:10.5194/acp-7-1213-2007, 2007.
- Sullivan, R. C., Moore, M. J. K., Petters, M. D., Kreidenweis, S. M., Roberts, G. C., and Prather, K. A.: Effect of chemical mixing state on the hygroscopicity and cloud nucleation properties of calcium mineral dust particles, *Atmos. Chem. Phys.*, 9, 3303–3316, doi:10.5194/acp-9-3303-2009, 2009.
- Swap, R., Garstang, M., Greco, S., Talbot, R., and Kallberg, P.: Saharan dust in the amazon basin, *Tellus*, 44, 133–149, 1992.
- Szyszkowski, B.: Experimental studies on capillary properties of aqueous solutions fatty acids, *Z. Phys. Chem.*, 64, 385–414, 1908.
- Tanaka, T. and Chiba, M.: A numerical study of the contribution of dust source regions to the global dust budget, *Global Planet. Change*, 52, 88–104, 2006.
- Tegen, I., Schepanski, K., and Heinold, B.: Comparing two years of Saharan dust source activation obtained by regional modelling and satellite observations, *Atmos. Chem. Phys.*, 13, 2381–2390, doi:10.5194/acp-13-2381-2013, 2013.
- Todd, M., Karam, D. B., Cavazos, C., Bouet, C., Heinold, B., Baldasano, J., Cautenet, G., Koren, I., Perez, C., Solmon, F., Tegen, I., Tulet, P., Washington, R., and Zakey, A.: Quantifying uncertainty in estimates of mineral dust flux: An intercomparison of model performance over the bodele depression northern chad, *J. Geophys. Res.*, 113, D24107, doi:10.1029/2008JD010476, 2008.
- Tost, H., Jöckel, P., Kerkweg, A., Sander, R., and Lelieveld, J.: Technical note: A new comprehensive SCAVenging submodel for global atmospheric chemistry modelling, *Atmos. Chem. Phys.*, 6, 565–574, doi:10.5194/acp-6-565-2006, 2006.
- Tulet, P., Crassier, V., Solmon, F., Guedalia, D., and Rosset, R.: Description of the mesoscale nonhydrostatic chemistry model and application to a transboundary pollution episode between northern france and southern england, *J. Geophys. Res.*, 108, D14021, doi:10.1029/2000JD000301, 2003.
- Tulet, P., Crassier, V., Cousin, F., Suhre, K., and Rosset, R.: ORILAM, a three moment lognormal aerosol scheme for mesoscale atmospheric model. on-line coupling into the mesonh-c model and validation on the escompte campaign, *J. Geophys. Res.*, 110, D18201, doi:10.1029/2004JD005716, 2005.
- Tulet, P., Grini, A., Griffin, R., and Petitcol, S.: ORILAM-SOA: A computationally efficient model for predicting secondary organic aerosols in 3-D atmospheric models, *J. Geophys. Res.*, 111, D19205, doi:10.1029/2006JD007152, 2006.
- Tulet, P., Mallet, M., Pont, V., Pelon, J., and Boone, A.: The 7–13 March, 2006, dust 1121 storm over West Africa: generation, transport and vertical stratification, *J. Geophys. Res.*, 113, D00C08, doi:10.1029/2008JD009871, 2008.
- Tulet, P., Crahan-Kahu, K., Leriche, M., Aouizerats, B., and Crumeyrolle, S.: Mixing of dust aerosols into a mesoscale convective system generation, filtering and possible feedbacks on ice anvils, *Atmos. Res.*, 96, 302–314, 2010.
- Twohy, C., Kreidenweis, S. M., Eidhammer, T., Browell, E., Heymsfield, A., Bansemer, A., Anderson, B., Chen, G., Ismail, S., DeMott, P., and van den Heever, S. C.: Saharan dust particles nucleate droplets in eastern atlantic clouds, *Geophys. Res. Lett.*, 36, 1129, doi:10.1029/2008GL035846, 2009.
- Wang, J., Cubison, M. J., Aiken, A. C., Jimenez, J. L., and Collins, D. R.: The importance of aerosol mixing state and size-resolved composition on CCN concentration and the variation of the importance with atmospheric aging of aerosols, *Atmos. Chem. Phys.*, 10, 7267–7283, doi:10.5194/acp-10-7267-2010, 2010.
- Washington, R., Todd, M., Engelstaedter, S., Mbainayel, S., and Mitchell, F.: Dust and the low-level circulation over the bodl depression, chad: Observations from bodex 2005, *J. Geophys. Res.*, 111, D03201, doi:10.1029/2005JD006502, 2006.
- Winker, D.: The CALIPSO mission, *B. Am. Meteorol. Soc.*, 91, 1211–1229, doi:10.1175/2010BAMS3009.1, 2010.
- Winker, D., Vaughan, M., Omar, A., Hu, Y., Powell, K., Liu, Z., Hunt, W., and Young, S.: Overview of the calipso mission and calip data processing algorithms, *J. Atmos. Oceanic Tech.*, 26, 2310–2323, 2009.
- Winker, D. M., Pelon, J., Coakley Jr., J. A., Ackerman, S. A., Charlson, R. J., Colarco, P. R., Flamant, P., Fu, Q., Hoff, R., Kit-taka, C., Kubar, T. L., LeTreut, H., McCormick, M. P., Megie, G., Poole, L., Powell, K., Trepte, C., Vaughan, M. A., and Wielicki, B. A.: The CALIPSO Mission: A Global 3-D View Of Aerosols And Clouds, *Bull. Amer. Meteor. Soc.*, 91, 1211–1229, doi:10.1175/2010BAMS3009.1, 2010.
- Wurzler, S., Reisin, T., and Levin, Z.: Modification of mineral dust particles by cloud processing and subsequent effects on drop size distribution, *J. Geophys. Res.*, 105, 4501–4512, 2000.
- Zender, C., Bian, H., and Newman, D.: Mineral Dust Entrainment and Deposition (DEAD) model: Description and global dust distribution, *J. Geophys. Res.*, 108, 4416, doi:10.1029/2002JD002775, 2003.